Toward the Accurate Prediction of Liquid Phase Oxidation of Aromatics: A Detailed Kinetic Mechanism for Toluene Autoxidation

Detlev Conrad Mielczarek, Mickaël Matrat, Arij Ben Amara, Yvan Bouyou, Perrine Wund, Laurie Starck

Toward the Accurate Prediction of Liquid Phase Oxidation of Aromatics: A Detailed Kinetic Mechanism for Toluene Autoxidation

Detlev Conrad Mielczarek, Mickaël Matrat,* Arij Ben Amara, Yvan Bouyou, Perrine Wund, and Laurie Starck

IFP Energies Nouvelles, 1 et 4 avenue de Bois-Préau, 92852 Rueil-Malmaison Cedex, France

ABSTRACT: Toluene is an important compound in the chemical industry as well as an often chosen simple surrogate compound for aromatic components in transport fuels. As a result, an improved understanding of the liquid phase oxidation of toluene is of interest to both the chemical industry and the transportation sector. In this work, a detailed autoxidation mechanism for the liquid phase oxidation of toluene is developed using an automated mechanism generation tool. The resultant mechanism is significantly improved using quantum chemistry calculations to update the thermodynamic parameters of key species in solution. Comparisons are made between the predicted and experimentally measured induction period and the obtained mechanism. The agreement between both is found to be within 1 order of magnitude. Rate of production analysis and sensitivity analysis are carried out to explain and understand the reactions paths present in the mechanism. The behavior of the mechanism is commented upon qualitatively; however, no quantitative data could be obtained with the selected test method.

1. INTRODUCTION

The liquid phase oxidation of toluene is a process that is applicable in many fields. For example, the process is employed in the chemical industries to produce commercially interesting compounds.[1,2] The same chemistry also applies to the thermal degradation of transport fuels, which are a complex mixture of many different types of hydrocarbons, each with their own properties and effects on the behavior of the fuel. Aromatics are naturally present in crude oil derived transport fuels. They ensure key properties such as octane number for gasoline fuels and seal swell and lubrication in jet fuels, but are also associated with the emission of more particulate matter from the engine postcombustion and implicated as possible precursors of deposit formation in fuel systems.[3−5]

The desire for more environmentally friendly fuel has driven research to understand the impact of fuel composition on fuel properties, to both enable an improved utilization of fuel, as well as to aid in the development of alternative fuels, which due to the long life of vehicles should ideally present a drop-in alternative.[6−8] One aspect of the fuel's properties is its thermal oxidative stability, which is known to be influenced by fuel composition.[9] To simplify the problem at hand for research purposes, surrogate fuels are often used to investigate the problem. In this work, toluene is chosen as one of the representatives for the aromatic species present in real fuels.[10,11]

Historically, pseudodetailed mechanisms that describe global kinetics and main oxidation pathways have been employed in the investigation of fuels.[12,13] However, their lumped nature precludes the elucidation of finer details in the behavior of the compound under investigation, such as for example the formation of oxidation products which may be responsible for deposit formation. Detailed mechanisms, such as those used for example in combustion[14] or more recently in the liquid phase,[15,16] offer an opportunity to gain greater insights into the individual steps including the identification of suitable precursors to deposit formation during the autoxidation process.[15,16]

The inherent complexity and size of such a detailed mechanism favor the use of automated tools[17] to aid in their development. Specifically, it enables the researcher to use a systematic approach in the construction of the mechanism based, considering all feasible reaction paths, while estimating suitable parameters using established theory. For example, Benson group additivity[18] is used to rapidly estimate the gas phase thermodynamic parameters of proposed structures, while kinetic parameters are proposed from known behavior and interactions of equal functional groups. Numerous tools exist for the generation of gas phase mechanisms and include ExGas and GENESYS.[17,19−22] We chose the Reaction Mechanism Generator (RMG) developed at MIT and Northeastern University,[23] with the main benefit being its support for liquid phase kinetics as well as its open source nature.

2. EXPERIMENTAL WORK

2.1. Oxidation Test Method and Experimental Conditions. The Anton Paar PetroOxy is a small scale static oxidation stability test rig, designed for the assessment of automotive fuels according to test methods ASTM D7545, D7525, and EN16091.[24] Advantages of the PetroOxy are its small sample volume which allows for the use of high purity solvents, the hard gold plated dish which should minimize catalytic reactions involving the reaction vessel, as well as the closed, well controlled nature of the test which minimizes outside influences. The main disadvantage of the PetroOxy is the requirement for a rigorous cleaning procedure to ensure good repeatability of the oxidation tests, which can be affected by trace contaminants. In addition, sampling can only be carried out after a test has been

completed. When the PetroOxy is utilized, a fuel sample is placed in a hard gold plated dish. The test chamber is then closed and pressurized with oxygen to 7×10^5 Pa, vented, and repressurized again to 7×10^5 Pa maximize the oxygen concentration in the pretest sample and test chamber. Next, the PetroOxy heats the test chamber, monitoring the headspace pressure during the entire process, which allows the user to follow the consumption of oxygen during the autoxidation process. A drop of 10% below the maximum pressure signifies the end of the test when using the standard test criteria, which is henceforth described as the induction period. The sample is then cooled to 20 °C (293.15 K), after which the PetroOxy depressurizes the test chamber. The stressed test sample may now be retained for further analysis or disposed of accordingly.

In this study, two types of PetroOxy measurements are employed. Single induction period runs at the three temperatures of 120 °C (393.15 K), 140 °C (413.15 K), and 160 °C (433.15 K) were carried out to identify the temperature dependence of the solvent oxidation process. A second measurement consisted of running the PetroOxy for additional pressure drop criteria of 20% and 40% to obtain a limited number of experimental data points over time as the sample is oxidized. The associated recorded pressure drops are included in Supplementary Figures B.10 and B.11.

After the test, the remaining liquid sample was transferred to a clear glass vial and stored in a refrigerator for further post-test analysis. The volume of the retained sample was assessed by photographing the vials under controlled conditions and calculating the recovered sample volume by comparing with reference volumes. Photos of the reference vials and samples retained in the 160 °C test series are shown in Supplementary Figures B.12 and B.13. Gas chromatography (GC) analysis was carried out to obtain data on the formation of oxidation products as well as toluene consumption and thus obtain some information about the initial development of oxidation products for our experimental work as well as to verify that we obtained the oxidation products reported in the literature.[1,2]

When nonstandard components are employed, be these jet fuels or in this case toluene, the same 10% pressure drop is observed and can be employed as a target condition for both experimental and modeling work, corresponding to a similar consumption of oxygen from the headspace. In earlier studies,[15,16] the 10% test criteria has been shown to correlate to a 5% consumption of the test fuel. However, for toluene it was found that at 120 °C (393.15 K), when taking the reduction in retained post test liquid sample volume into account, around 48% of the initial toluene sample is consumed, while at 140 °C (413.15 K) around 46% is consumed. Finally, at 160 °C (433.15 K), around 43% of the initial toluene sample is consumed at the 10% pressure drop criteria. These values are therefore used as comparison targets for the so-called induction period in this work. For the 20% pressure drop criteria at 160 °C (433.15 K) around 53% of the sample was found to have been consumed, while 82% of the toluene sample was consumed for the 40% criteria at the same temperature. In addition, tests have shown that reproducibility with solvents is significantly better than with real fuels with errors of around ±1.5% in the measurement of the induction period.[15,16,25]

2.2. Oxidation Products Analysis Techniques. Species were identified in undiluted samples by applying gas chromatography mass spectrometry using an Agilent 5975C inert XL mass spectrometer with a 7890 gas chromatograph and a PONA column of 50 m length, 200 μm diameter, and 0.5 μm film thickness. The carrier gas was helium, and the temperature profile consisted of an initial temperature of 35 °C (308.15 K) for 5 min, followed by a temperature rise to 70 °C (343.15 K) at a rate of 1 °C min^{-1} (1 K min^{-1}). Finally, the temperature was raised at a rate of 4 °C min^{-1} (4 K min^{-1}) to 325 °C (598.15 K), holding the final temperature for 1.25 min.

The overall strategy for the quantification consisted of using a similarly configured gas chromatography mass spectrometer and a gas chromatography flame ionization detector. The gas chromatography mass spectrometer enabled the identification of oxidation products, while the gas chromatography flame ionization detector enabled the quantification of oxidation products. This work employed an Agilent 6890N gas chromatograph using a DB-FFAP column of 60 m length,

250 μm diameter, and 0.25 μm film thickness coupled to a 5973 mass spectrometer. The quantification with a flame ionization detector was carried out on an Agilent 6890N gas chromatograph using the same DB-FFAP column as the gas chromatography mass spectrometer. The temperature profile used consisted of an initial temperature of 60 °C followed by a 10 °C min^{-1} (10 K min^{-1}) temperature rise to 150 °C (423.15 K). This was followed by a 25 °C min^{-1} (25 K min^{-1}) temperature rise to 250 °C (523.15 K). The flame ionization detector was used at a temperature of 200 °C (473.15 K). A total of 0.2 μL of the sample was injected in split mode, using a 500/1 split ratio.

The quantification employed acetonitrile from VWR with a purity of 99.95% as an internal standard. A calibration curve was obtained for toluene, 99.8%, anhydrous from Sigma-Aldrich, with concentrations from 3% to 14% and a 1% acetonitrile concentration level by mass. The quantitative analysis was carried out on samples using a blend of around 1% acetonitrile, 4% of the sample under investigation, and 95% ethanol by mass.

3. MODELING APPROACH

The modeling approach in this study covers the following main steps. First, a core mechanism is generated with RMG, which is then extended by adding termination reactions. Next, the mechanism is improved with the help of quantum chemistry calculations. Finally, the mechanism is analyzed in greater detail using methods such as global brute force sensitivity analysis to obtain an improved understanding of its behavior.

3.1. Background. *3.1.1. Reaction Mechanism Generator.* The RMG is an automated code designed to propose chemical kinetics mechanisms for both gas and liquid phase conditions, based on a number of initial conditions.[15,16,23,26,27] These include the initial reactant species, their structure and concentration, the temperature, as well as, in the case of a liquid phase model, the solvent used. It has previously been employed successfully for the simulation of the liquid phase oxidation of C_8 to C_{16} normal alkanes[16] as well as fatty acid methyl ester blends[15] and is applied to toluene in this study.

The generation of a mechanism covers the identification of possible reactions with appropriate parameters as well as the estimation of appropriate thermodynamic data. For the identification of possible reactions, RMG employs a library of reaction types, such as radical recombinations as well as hydrogen abstractions with relevant kinetic parameters, for defined molecular graphs. For every molecule in the mechanism, possible reactions from the library, based on the structural information of the molecule are tested. The "best" candidate reactions, based on reaction flux, are automatically selected for use in the model. Where no data are present for a reaction, related parameters are averaged to obtain an estimate for the reaction in question. As RMG was initially designed to model combustion kinetics, corrections were introduced to enable the simulation of liquid phase conditions.[28−30] These corrections are applied to both the thermodynamic parameters of species as well as the kinetic parameters and are dependent on both the solvent and the solute. In RMG, two corrective methods are employed for the thermochemistry. The Gibbs energy of solvation is estimated using a "linear solvation energy relationship" (LSER)[31,32] which presents a parametrized description of solvent effects. This method takes aspects such as viscosity and polarity into account as well as descriptions of the solute, for example, the presence of methyl groups. In general, the LSER approach has been shown to provide a good accuracy for most solvents[29,30] at low computational cost. The second corrective method employed in RMG is the Mintz model[33−36] for the enthalpy of formation, which aims to

describe the liquid phase enthalpy of formation. The Mintz model uses a similar parametrization approach when compared to the LSER approach for the Gibbs energy of solvation. Published enthalpies of formation for closed shell species in the liquid phase were collected by Mintz et al.[33−36] for a large number of solvents and solutes to derive an expression which describes the enthalpy of solvation in the liquid phase. This then allows the derivation of the liquid phase enthalpy of formation from a known gas phase enthalpy of formation. The remaining thermodynamic parameter, the liquid phase entropy, is calculated by RMG from the Gibbs free enthalpy in solution as well as the enthalpy of formation in solution. On the kinetic side, RMG ensures that reactions do not exceed their diffusion limit.[37,38] This is achieved by estimating an "effective rate constant" that takes into account the radii of the involved molecules as well as the diffusion rates in the solvent. In RMG 1.0.4, due to a numerical problem, a constant limit for the diffusion term, irrespective of the solute, is applied.[39] A fix, available in newer RMG releases, was backported for the mechanism generation process. No significant difference in the mechanism was observed, due to the slow nature of the bimolecular reactions in the reaction mechanism.

3.1.2. Quantum Chemistry Background. Quantum chemical calculations have been established as a valuable tool when investigating the behavior of novel compounds or of compounds that are hard to investigate using experimental methods, be it due to costs restraints or due to the short lifespan of the species. One use of quantum chemical calculation is the determination of thermodynamic parameters, such as can be used in a chemical kinetics mechanism. In the context of this study, this calculation was performed to assess and improve the quality of the RMG-predicted thermodynamic parameters for individual species in the liquid phase.

The most commonly used methods for calculating molecular properties are CCSD(T) as well as CBS methods, as these methods theoretically promise the greatest accuracy, albeit at a large computational cost. As an example, many entries in the RMG kinetics database were obtained with CBS-QB3.[23,29,30] Other methods used in benchmarks are the Gx methods in the Gaussian suite as well as W1 methods.[40−46] A more accessible approach in the study of a large number of compounds is to choose a computationally lighter method.[47] Density functional theory offers improved accuracy relative to semiempirical methods, while not commanding the computational costs of couple cluster computations, commonly employed in the calculation of reference values. Since their introduction, density functionals have seen continuous development as well as accuracy improvements relative to benchmark methods, making them a readily accessible quantum chemical tool.[48] One of the most common methods used in the application of quantum chemistry is the well established B3LYP functional with variations of the 6-31G/6-311G basis set, for example, in the investigation in jet fuel as well as toluene autoxidation.[2,49−52] However, a recent paper argued that "pure" B3LYP should not be used for thermochemical calculations without newer corrective methods, such as a geometric counterpoise correction and London dispersion correction, based on an assessment across the GMTKN30 benchmark data set.[53] Additionally, general benchmarks as well as a large number of comparison studies in the field of organic chemistry have shown that the overall performance of B3LYP is lower than the performance of newer functionals which are thus more advisable.[40,54−61]

The functional chosen in this study is M06-2X which offers broad applicability to many different chemical systems and has proven its capabilities in terms of accuracy since, including in the application to organic chemistry.[57−59,62−65] Together with a modern Ahlrich's basis set[66] and the RI-J[67] auxiliary basis set, density functional theory (DFT) offers the opportunity to comparatively rapidly calculate and evaluate a large number of compounds with reasonable accuracy.[68] In the GMTKN30 benchmark of 2011, M06-2X performed best for basic properties with a weighted total mean absolute deviation of 3.2 kcal/mol and is one of the best performing hybrid functionals.[68] Solvation is considered using the SMD model,[69] which has been shown to perform well when compared to other implicit solvation models and may potentially only be outperformed by COSMO-RS which is not widely available.[70,71] Explicit solvation may provide more accurate predictions of properties;[72] however, such a calculation is beyond the scope of this study.

3.2. Generation Steps. *3.2.1. Core Mechanism Generation in RMG.* The version of RMG employed in this study belongs to the 1.0.4 branch, with the Git hashes given in Supplementary Data A.1. As this study focuses on a small experimental test rig, the PetroOxy, initial input conditions in RMG were chosen to reasonably represent the experimental conditions. With experimental data collected from 120 to 160 °C (393.15−433.15 K), simulation temperatures of 400, 450, and 500 K were chosen, with the higher 500 K criteria selected to capture reactions expected at slightly elevated temperatures. Initial oxygen concentrations were chosen to represent the expected air saturated concentration of oxygen under standard conditions, which is around 1000 ppm according to Henry's constant quoted by Denisov[73] as 9.88×10^{-3} mol L^{-1} atm^{-1}. Using Henry's Law,[74] the expected value when pressurized to 1.17×10^6 Pa at normal temperature is closer to 10 000 ppm, while 100 ppm is closer to quoted oxygen concentrations in transport fuels during use and in standard storage conditions.[75] To favor model convergence in RMG, boundary conditions, such as maximum oxygen and carbon atoms per species, were added in the input file.

3.2.2. Mechanism Extension in RMG. Termination reactions are key reactions in autoxidative processes in the literature, which supports their inclusion in the mechanism.[12,13,73] Limiting the number of carbon atoms in the RMG mechanism aids convergence; however, it precludes the consideration of termination species. In addition, computational requirements can become prohibitive if the model is not sufficiently constrained. Therefore, termination reactions were obtained using a dedicated mechanism generation run and added to the base model, as discussed in Section 3.2. Termination reactions were separately generated in a dedicated RMG mechanism and merged with the initially generated mechanism to produce an enhanced mechanism in accordance with current literature.[73] This follows the previously developed methodology by Ben Amara et al.[15] and Chatelain et al.[16]

3.2.3. Mechanism Improvement using Quantum Chemistry. The model was improved with the help of quantum chemistry calculations, which were carried out to estimate new thermodynamic data for key species involved in the model. This covers the small oxygenated species as well as oxygen, toluene, and all primary oxidation products found in the model, giving a total of 45 species. An overview of number of species updated in each category in the final model is shown in Table 2. The details of choosing the "right" functional and basis set are

Table 1. Overview over the Generation Setup as Employed in RMG (Top) as well as the Chemical Kinetics Simulation Conditions (Bottom)

temperature (K)	400/450/500
pressures (atm)	268.03/273.80/278.80
toluene concentration	9.442×10^{-3} mol cm^{-3}
oxygen concentration	$9.442 \times 10^{-5}/10^{-6}$ mol cm^{-3} (constant)
temperature (K)	393.15/413.15/433.15
pressures (atm)	268.03/273.80/278.80
toluene fraction	0.9879
oxygen fraction	0.0121 (constant)

discussed in Section 3.3.1, while the details of calculating the thermodynamic parameters is calculated in Section 3.3.2.

Table 2. Overview of Species for which new Thermochemistry Parameters are Calculated

species type	count
toluene, oxygen	2
"small oxygenated species"	4
"alkyl species"	4
"oxyl radicals"	4
"peroxyl species"	4
alcohols	4
hydroxides	4
benzaldehyde	1
benzoic acid and intermediates	5

The thus obtained improved mechanism was compared to experimental data obtained from a PetroOxy. A criterion of fuel consumption, in this case toluene, was used as the criteria to define an "induction period", which has been shown to correspond to a 5% fuel consumption for n-alkanes[15,16] and to be around 43−48% fuel consumption for toluene in this work.

3.3. Quantum Chemistry. *3.3.1. Selection of Method/ Functional and Basis Set.* In this work, quantum chemistry calculations were carried out using the quantum chemistry package ORCA.[76] The M06-2X functional is used with the def2-TZVP basis set in conjunction with the def2-TZVP/J auxiliary basis set.[66,67] Because of the known mesh dependence of the Minnesota functionals,[68] finer grids were employed for both the optimization of the molecule as well as the final energy calculation. Every species was optimized, prior to the frequency calculations being carried out, which verified that the species found was stable and also predicted the temperature dependence of relevant species properties. The input header is shown in Appendix A.1. The default parameters were employed for the SMD solvation model, setting the solvent simply to toluene.

The calculated enthalpies of formation in the gas phase for a selection of key species in the autoxidation of toluene using M06-2X and ωB97X-D3 with def2-TZVP, def2-TZVP/J, as well as B3LYP with 6-31G* is shown in Table 3. Calculations were carried out using reported enthalpies of formation from NIST.[77] Alternatively where no or not very accurate reference data are available, such as for the benzyl radical, the calculated enthalpies were used. Values from a recent paper[42] are provided as an added reference to assess the quality of calculated enthalpies of formation. As can be seen in Table 3, B3LYP in the commonly used combination with 6-31G* performs badly,

with an error of up to around 50 kJ/mol for the benzyl radical, while both M06-2X and ωB97X-D3 predict values more in line with available data. The disparity between calculated values in different isodesmic reactions is also largest in B3LYP, most visible with the hydroperoxide ROOH. In contrast, overall, M06-2X and ωB97X-D3 perform very similar with the largest difference observed in the prediction of the enthalpy of formation for the hydroperoxide. Overall the use of M06-2X results in more values that are more in line with values from the literature.[42] Thus M06-2X was chosen as the preferred functional in this study. The shorter compute times relative to ωB97X-D3 are a further benefit. Nevertheless, it should be pointed out that the good performance of the highly parametrized M06-2X is very likely related to the compounds studied in this work, which are related to the training set used in the parametrization of the functional.

A common method to calculate enthalpies of formation uses isodesmic reactions,[78,79] in which reference molecules are employed for the calculation of the enthalpy of formation.[80,81] The impact of solvation is modeled using the highly parametrized SMD model with toluene as the solvent, as it promises the best performance of the available implicit solvation models in ORCA.[69,76] All geometries were reoptimized with the solvation models, and frequency calculations carried out with the solvation model enabled the capture of the solvent effects relative to the gas phase molecule. The optimized *xyz* geometries for the molecules in the gas phase and with the SMD model applied are included in the Supplementary Data Section C.3.

3.3.2. Calculating Thermodynamic Parameters for the Liquid Phase. The thermodynamics of solvation are commonly expressed as a relationship in the Gibbs free enthalpy of solvation between the compound in the gas phase and as a solute.[23,32,69] A common aspect in this method is the use of identical units for both the gas phase, as well as the liquid phase. For example, the SMD model has been developed and parametrized assuming that calculations in both the gas and liquid phase use a mol/L concentrations descriptor.[69] The same approach applies to the Abraham LSER approach.[32] When calculations are carried out in ORCA, the output is presented for the standard gas phase condition of 1 atm and 298.15 K in both gas phase and liquid phase calculations.[76] To obtain values in useful units for the liquid phase, it becomes thus necessary to compress the molecule in the gas phase state from 1 atm at 298.15 K to 1 mol/L at 298.15 K. The work or energy required for the isothermal expansion is described by eq 1.[74]

$$w = -nRT \int_{V_i}^{V_f} \frac{1}{V} \, dV = -nRT \, \ln\left(\frac{V_f}{V_i}\right) \tag{1}$$

With the standard condition of 298.15 K at 1 atm, the volume changes from 24.5 to 1 L for a liquid phase reference state with mol/L units, resulting in an energy cost of 1.895 kcal/mol.[82] As thermodynamic data in a liquid phase model should apply to the liquid phase condition, ideally being comparable to experimental values, this term is included in the form of $G_{compression}$ in the thermodynamic data calculation carried out with ORCA.[76]

To calculate the enthalpy of formation in the liquid phase, $\Delta H_{f\,liquid}$, shown in eq 3, one can use the definition for the Gibbs free enthalpy, shown rearranged in eq 4 to obtain the entropy in the liquid phase S_{liquid}, shown in eq 5.[82] Equation 5 can be contracted with the help of eq 3 into eq 6. Calculating

Table 3. Calculated Enthalpies of Formation in the Gas Phase in kJ/mol for the Evaluation of the Functional of Choice[a]

		all ΔHf in kJ/mol		M06-2X		WB97X-D3		B3LYP		Sandhyia[42]	
		NIST[77]		def2-TZVP		def2-TZVP		6-31G*		Theo.	Exp.
		ΔH_f	isodesmic reaction	$H\,E_h$	ΔH_f	$H\,E_h$	ΔH_f	$H\,E_h$	ΔH_f	ΔH_f	ΔH_f
S1	O2t	0		−150.31999621		−150.33920544		−150.24957557			
S11	HO	38.99		−75.72055732		−75.73109668		−75.67664251		35.9	37.5
S12	H₂O	−241.83		−76.40080953		−76.41349784		−76.34499855		−243.9	−241.8
S13	HO₂	2.09	S13+S12 = S14+S11	−150.8900051	13.7	−150.91132477	2.1	−150.81435539	10.8	15.5	12.3
S14	H₂O₂	−136.11	S14 = S11+S11	−151.52035277	−130.1	−151.53942146	−124.8	−151.43171421	−127.9	−136.3	−135.4
S15	CH₃	145.69		−39.79034067		−39.80541077		−39.77137715			
S16	CH₄	−74.6 ± 0.31		−40.4514246		−40.47075045		−40.432677			
S17	CH₂O	−115.9		−114.46840382		−114.48506455		−114.40832031			
S51	phenyl	339 ± 8	S51+S15 = S101	−231.44577585	333.4	−231.47462905	334.1	−231.31277011	321.6		
S101	toluene	50.1 ± 1.1		−271.39951965		−271.4436911		−271.2430399		52.6	50.4
S102	benzyl	207 ± 4	S102+S16 = S101+S15	−270.7610411	211.0	−270.80302447	205.6	−270.58741439	255.5	225.7	208.0
S103	ROJ		S102+S12 = S104+S11	−345.95569926	125.9	−346.003275	125.3	−345.76289334	125.8	126	136
			use calc. ROH		125.6		127.5		136.3		
S104	ROH	−94.6 ± 3	S104 = S102+S11	−346.61296542	−94.9	−346.66247474	−92.4	−346.40822284	−84.0	−95.5	−94.6
											−88.8
S105	ROOJ		S105 = S102+S1	−421.11542339	120.8	−421.1714378	128.9	−420.8864465	125.6	123.8	114.6
S106	ROOH		S106 = S102+S13	−421.74374965	−34.3	−421.79762982	−9.6	−421.50206519	−54.2	−28.5	
			use calc. HO₂		−22.7		−9.5		−45.5	−21	
			use calc. benzyl		−30.3		−11.0		−5.7		
			use calc. benzyl, HO₂		−18.7		−10.9		3.0		
			S106+S12 = S104+S14		−18.4		−13.1		−7.6		
			use calc. ROH		−18.7		−16.2		−7.8		
			S106 = S102+S13		−34.3		−9.6		−54.2		
			use calc. HO₂		−22.7		2.0		−42.6		
			use calc. benzyl		−30.3		−5.5		−50.2		
			use calc. benzyl, HO₂		−18.7		6.1		−38.6		
S107	R = O	−36.8 ± 3.0	S107+S16 = S101+S17	−345.43687597	−44.7	−345.47852463	−45.1	−345.24316373	−55.5	−39.8	−36.7
			S107+S15 = S102+S17		−44.7		−45.1		−55.5		

[a]In the calculation, either values from NIST or from the quantum chemistry calculation are employed. Def2-TZVP is employed with def2-TZVP/J auxilliary basis set, B3LYP is the ORCA implementation.

the liquid phase entropy from the Gibbs free enthalpy and the enthalpy of formation avoids the problem of calculating the liquid phase entropy, which would ideally require a molecular dynamics simulation and is beyond the scope of this work.[72]

$$G_{liquid} = G_{gas} + G_{solvation} + G_{compression} \quad (2)$$

$$\Delta H_{f\,liquid} = \Delta H_{f\,gas} + \Delta H_{solvation} \quad (3)$$

$$T \times S_{liquid} = H_{f\,liquid} - G_{liquid} \quad (4)$$

$$T \times S_{liquid} = \Delta H_{f\,liquid} - (\Delta H_{f\,gas} - T \times S_{gas} + G_{solvation} + G_{compression}) \quad (5)$$

$$T \times S_{liquid} = \Delta H f_{solvation} + T \times S_{gas} - (G_{solvation} + G_{compression}) \quad (6)$$

When energies are calculated using an isodesmic reaction, an arbitrary theoretical reaction in which the same types of bonds are broken and formed is described.[44,78,83] For example, a hydrogen can be migrated from the methyl group in toluene to a methyl radical molecule to create the benzyl radical and methane, as shown in eq 7. The same methodology can be expanded to any other compound for which a reaction with only one unknown species can be formulated. With this technique, accurate enthalpies of formation for the reference compounds are required to minimize the final error.

As a specific example, let us look at the calculation of the enthalpy of formation for the benzyl radical. Reference data from NIST[77] as well as the quantum chemistry calculation in ORCA[76] are given in Table 3, using the data from M06-2X. We can formulate the formation of the benzyl radical using the following reaction, shown in eq 7:

$$RH\,(toluene) + R\cdot(methyl)$$
$$\rightarrow R\cdot(benzyl) + RH\,(methane) \quad (7)$$
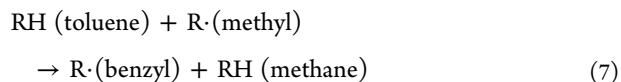
Substituting the calculated enthalpies and then rearranging to solve for the benzyl radical, we obtain an enthalpy of formation of roughly 211 kJ/mol, which falls into the uncertainty of the reference data and also falls between the theoretical and experimental data presented in a recent publication.[42] The uncertainty in the example calculation is up to ±1.41 kJ/mol before considering any uncertainties in the accuracy of the quantum chemistry calculation.

This methodology has been applied to all primary oxidation products as well as intermediate species in the formation of benzoic acid. Thermodynamic parameters for oxygen, toluene, and small oxygenated species in solvation were calculated from literature values, except HO₂· for which literature values differ and which was therefore calculated.[42,77] Thus we have an autoxidation mechanism for toluene, in which 32 species have received thermodynamic data that was updated using quantum chemistry calculations, while a further 141 species, both secondary oxidation products and termination species, retained
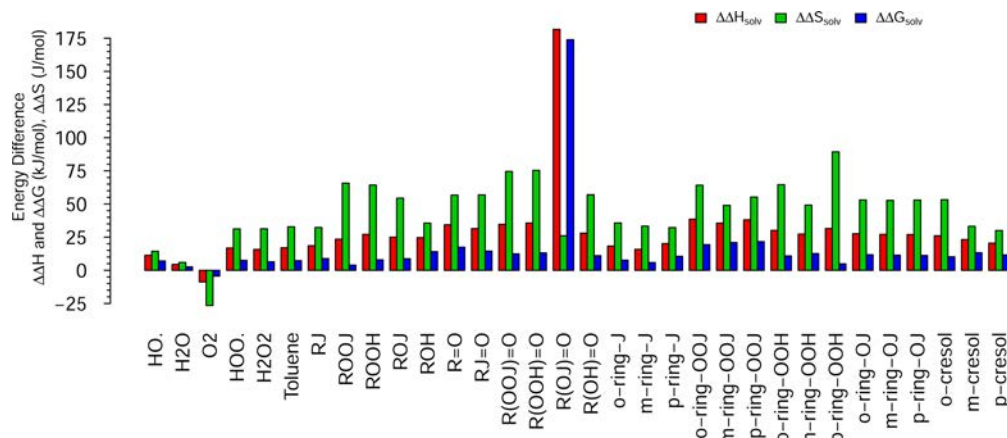
Figure 1. Plot of the difference in the solvation enegies between RMG and the quantum chemistry calculations from Table 5 in which a correction to the Gibbs enthalpy of solvation is applied. $\Delta\Delta H_{f\,solv}$ and $\Delta\Delta G_{solv}$ are in kJ/mol while $\Delta\Delta S_{fsolv}$ is in J/(mol K).

Table 4. Calculated Thermodynamic Data from RMG, with Values Quoted for the Reference Temperature of 298.15 K

	gas phase			liquid phase			solvation		
molecule	ΔH_f kJ/mol	S_f J/(mol K)	ΔG kJ/mol	ΔH_f kJ/mol	S_f J/(mol K)	ΔG kJ/mol	ΔH_{solv} kJ/mol	ΔS_{solv} J/(mol K)	ΔG_{solv} kJ/mol
HO.	37.07	183.93	−17.77	16.07	143.09	−26.60	−21.00	−40.84	−8.83
H₂O	−241.84	188.61	−298.07	−258.49	156.19	−305.06	−16.65	−32.43	−6.98
O2t	0.00	205.10	−61.15	0.00	205.10	−57.66	0.00	0.00	3.49
HOO.	12.55	229.07	−55.75	−19.71	171.33	−70.79	−32.26	−57.74	−15.04
H₂O₂	−135.90	234.51	−205.82	−168.20	176.77	−220.90	−32.30	−57.74	−15.09
toluene	49.41	327.15	−48.13	8.95	267.36	−70.76	−40.46	−59.79	−22.63
RJ	201.71	310.66	109.09	161.80	251.71	86.75	−39.92	−58.95	−22.34
ROOJ	124.06	403.13	3.86	63.51	311.88	−29.47	−60.54	−91.25	−33.34
ROOH	−26.99	402.21	−146.91	−87.49	310.95	−180.20	−60.50	−91.25	−33.29
ROJ	122.63	365.56	13.64	68.78	284.85	−16.14	−53.85	−80.71	−29.78
ROH	−94.77	371.66	−205.58	−148.62	290.96	−235.36	−53.85	−80.71	−29.78
R = O	−44.81	348.32	−148.66	−98.53	265.47	−177.68	−53.72	−82.84	−29.02
RJ = O	109.58	353.00	4.33	55.15	269.53	−25.22	−54.43	−83.47	−29.55
R(OOJ)=O	−40.58	425.89	−167.56	−106.69	324.93	−203.57	−66.11	−100.96	−36.01
R(OOH)=O	−234.01	424.97	−360.72	−300.12	324.01	−396.72	−66.11	−100.96	−36.01
R(OJ)=O	−94.60	376.23	−206.77	−300.12	324.03	−396.73	−205.52	−52.20	−189.95
R(OH)=O	−311.75	372.92	−422.94	−369.20	289.66	−455.56	−57.45	−83.26	−32.62
O-ring-J	304.22	333.34	204.83	263.22	273.05	181.81	−41.00	−60.29	−23.03
m-ring-J	304.22	333.34	204.83	263.47	273.30	181.98	−40.75	−60.04	−22.85
p-ring-J	304.22	333.34	204.83	263.30	273.13	181.86	−40.92	−60.21	−22.97
p-ring-OOJ	121.55	395.93	3.50	61.50	305.39	−29.55	−60.04	−90.54	−33.05
m-ring-OOJ	121.55	395.93	3.50	61.50	305.39	−29.55	−60.04	−90.54	−33.05
p-ring-OOJ	121.55	395.93	3.50	61.50	305.39	−29.55	−60.04	−90.54	−33.05
O-ring-OOH	−29.50	395.01	−147.27	−89.54	304.47	−180.32	−60.04	−90.54	−33.05
m-ring-OOH	29.50	395.01	−88.28	−89.54	304.47	−180.32	−60.04	−90.54	−33.05
p-ring-OOH	−29.50	395.01	−147.27	−89.54	304.47	−180.32	−60.04	−90.54	−33.05
O-ring-OJ	23.47	353.34	−81.88	−29.37	274.14	−111.11	−52.84	−79.20	−29.23
m-ring-OJ	23.47	353.34	−81.88	−29.58	273.93	−111.25	−53.05	−79.41	−29.38
p-ring-OJ	23.47	353.34	−81.88	−29.29	274.26	−111.06	−52.76	−79.08	−29.18
o-cresol	−126.73	357.98	−233.47	−180.41	278.91	−263.57	−53.68	−79.08	−30.10
m-cresol	−126.73	357.98	−233.47	−180.41	278.91	−263.57	−53.68	−79.08	−30.10
p-cresol	−126.73	357.98	−233.47	−180.41	278.91	−263.57	−53.68	−79.08	−30.10

their RMG thermodynamic data. The breakdown of the 32 key species is shown in Table 2 and covers small oxygenated species as well as the initial reactants and primary oxidation products. Comparing the estimated thermodynamic parameters from RMG in both the gas phase and the liquid phase with the calculated values from the quantum chemistry calculations reveals good agreement in the gas phase, as would be expected given the gas phase heritage of the RMG code. While there are some differences in the predicted enthalpy of formation and entropy, these are generally small. However, when comparing the thermodynamic parameters for the liquid phase, the divergence between the predictions from RMG and the quantum chemistry calculations becomes more significant in both the enthalpy and entropy. To maintain a consistent

Table 5. Calculated Thermodynamic Data from Quantum Chemistry, Including a Correction to the Gibbs Enthalpy of Solvation, with Values Quoted for the Reference Temperature of 298.15 K

molecule	gas phase			liquid phase			solvation			(QC value) − (RMG value)		
	ΔH_f kJ/mol	S_f J/(mol K)	ΔG kJ/mol	ΔH_f kJ/mol	S_f J/(mol K)	ΔG kJ/mol	ΔH_{solv} kJ/mol	ΔS_{solv} J/(mol K)	ΔG_{solv} kJ/mol	$\Delta\Delta H_{f\ solv}$ kJ/mol	$\Delta\Delta S_{solv}$ J/(mol K)	$\Delta\Delta G_{solv}$ kJ/mol
HO.	38.99	172.38	−12.41	29.29	145.88	−14.20	−9.70	−26.50	−1.80	11.31	14.33	7.03
H_2O	−241.83	185.16	−297.04	−254.06	158.68	−301.37	−12.23	−26.48	−4.33	4.43	5.95	2.65
O_2	0.00	204.62	−61.01	−8.77	178.09	−61.87	−8.77	−26.54	−0.86	−8.77	−26.54	−4.35
HOO.	13.69	219.22	−51.68	−1.79	192.69	−59.24	−15.47	−26.53	−7.56	16.78	31.21	7.48
H_2O_2	−136.11	222.82	−202.54	−152.67	196.35	−211.21	−16.56	−26.47	−8.66	15.75	31.27	6.42
toluene	50.10	314.75	−43.74	26.67	287.76	−59.12	−23.43	−26.99	−15.38	17.03	32.80	7.25
RJ	211.04	310.68	118.41	189.64	283.99	104.97	−21.40	−26.69	−13.44	18.52	32.26	8.90
ROOJ	125.82	360.38	18.37	88.74	334.84	−11.09	−37.08	−25.55	−29.46	23.47	65.71	3.87
ROOH	−30.26	359.46	−137.44	−63.65	332.52	−162.79	−33.38	−26.94	−25.35	27.12	64.32	7.94
ROJ	125.60	337.48	24.97	96.72	311.15	3.95	−28.87	−26.33	−21.02	24.98	54.38	8.76
ROH	−94.87	340.48	−196.39	−124.07	295.34	−212.12	−29.19	−45.14	−15.74	24.65	35.57	14.05
R=O	−44.70	323.83	−141.25	−64.12	297.72	−152.88	−19.42	−26.11	−11.63	34.31	56.73	17.39
RJ=O	126.53	329.68	28.24	103.52	303.09	13.15	−23.01	−26.59	−15.09	31.42	56.88	14.46
R(OOJ)=O	−19.39	367.25	−128.89	−50.87	340.84	−152.50	−31.48	−26.42	−23.60	34.63	74.54	12.40
R(OOH)=O	−208.07	362.57	−316.17	−238.54	336.98	−339.01	−30.48	−25.59	−22.85	35.63	75.37	13.16
R(OJ)=O	−37.55	348.69	−141.52	−61.44	322.56	−157.61	−23.89	−26.14	−16.09	181.63	26.06	173.86
R(OH)=O	−301.25	339.86	−402.58	−330.67	313.62	−424.18	−29.42	−26.24	−21.60	28.02	57.02	11.02
O-ring-J	305.86	323.26	209.48	283.10	298.71	194.04	−22.76	−24.55	−15.44	18.24	35.74	7.59
m-ring-J	307.67	321.54	211.81	282.70	294.81	194.80	−24.98	−26.73	−17.01	15.77	33.31	5.84
p-ring-J	305.59	321.84	209.63	284.81	293.82	197.21	−20.78	−28.02	−12.42	20.14	32.19	10.55
p-ring-OOJ	101.94	360.72	−5.61	80.42	334.31	−19.25	−21.51	−26.41	−13.64	38.53	64.14	19.40
m-ring-OOJ	102.85	364.85	−5.93	78.36	323.29	−18.03	−24.49	−41.56	−12.10	35.55	48.98	20.94
p-ring-OOJ	103.56	374.18	−8.00	81.60	338.87	−19.44	−21.96	−35.31	−11.44	38.08	55.23	21.61
O-ring-OOH	−45.07	354.02	−150.63	−75.01	328.10	−172.83	−29.93	−25.93	−22.20	30.11	64.62	10.84
m-ring-OOH	−43.68	359.47	−150.85	−76.42	318.07	−171.26	−32.75	−41.40	−20.40	27.29	49.14	12.64
p-ring-OOH	−43.36	344.75	−146.15	−71.89	343.53	−174.31	−28.53	−1.22	−28.16	31.51	89.32	4.88
O-ring-OJ	26.19	338.19	−74.64	0.93	312.04	−92.10	−25.26	−26.15	−17.46	27.59	53.05	11.77
m-ring-OJ	27.43	327.25	−70.14	1.47	300.61	−88.15	−25.95	−26.64	−18.01	27.10	52.77	11.37
p-ring-OJ	28.17	342.88	−74.06	2.36	316.75	−92.08	−25.80	−26.13	−18.01	26.96	52.95	11.17
o-cresol	−132.04	334.51	−231.77	−159.67	308.63	−251.69	−27.64	−25.88	−19.92	26.04	53.20	10.18
m-cresol	−129.56	343.73	−232.05	−160.09	297.83	−248.89	−30.53	−45.90	−16.85	23.15	33.18	13.26
p-cresol	−126.84	346.39	−230.11	−159.98	297.30	−248.63	−33.15	−49.09	−18.51	20.53	29.99	11.59

mechanism, updates to the thermodynamic data were applied to all species in the dominant reaction pathway. Plots for the species representing the dominant reaction route are shown in the Supplementary Data section C.2.1. For the standard condition of 298.15 K, the comparison between the calculated quantum chemistry value is shown in Figure 1. The calculated values for the thermodynamic data in RMG are shown in Table 4, while the calculated values for the quantum chemistry calculation and their difference relative to the RMG values is shown in Table 5.

As can be seen from Figure 1, overall agreement between the quantum chemistry calculation and RMG is good for the Gibbs free enthalphy for all but one species, the radical formed in the decomposition of the hydroperoxide group in the perbenzoic acid. The comparatively constant deviation in the Gibbs free enthalpy between RMG and the quantum chemistry calculations is the result of RMG not taking the transition from the gas phase reference state to the liquid phase reference state into account. One can further observe that RMG consistently predicts lower enthalpies of formation as well as lower entropies when compared to quantum chemistry calculations, except for oxygen. Inspection of Table 4 also shows that RMG is not able to predict thermodynamic differences in between

isomers, such as for example the three cresol isomers. While these are known to have slightly differing enthalpies of formation, and these differences are reflected in the quantum chemistry calculations, the RMG-predicted enthalpies of formation are identical. The same is true for the corresponding alkyl radical, peroxyl radical, hydroperoxide and oxyl radical species.

3.4. Sensitivity Analysis and 0D Chemical Kinetics.
Brute force sensitivity analysis can provide insights into the response of a chemical kinetics mechanism to minor or major changes in the Arrhenius parameters. This method can be employed to probe the mechanism's sensitivity to minor changes and offers the user the ability to identify reaction whose parameters exhibit a significant impact on the mechanism behavior and thus warrant a further investigation. Brute force sensitivity analysis was carried out by developing a simple dedicated C++ code to read the chemkin input file generated by RMG and write output files with adjusted Arrhenius parameters using a systematic naming pattern based on user defined parameters. In a second step, Bash with the option of GNU parallel[84] may be employed to solve the modified mechanisms using a solver of choice. The data are post processed using R,[85] and the result is reported as a

percentage change in the induction time, t, of the modified mechanism relative to the unmodified mechanism using the method in eq 8.

$$\%t_{\text{change}} = \frac{(t_{\text{modified}} - t_{\text{original}})}{t_{\text{original}}} \times 100\% \tag{8}$$

Where the temperature dependence is investigated, the output is presented as the absolute change in the temperature dependence of the induction time when comparing the original and modified mechanism, shown in eq 9.

$$\text{output} = \frac{\mathrm{d}}{\mathrm{d}T}\log_{10}(t_{\text{modified}}) - \frac{\mathrm{d}}{\mathrm{d}T}\log_{10}(t_{\text{original}}) \tag{9}$$

For 0D chemical kinetics, this study employed an in-house solver, Cloe,[16,86] as it is able to simulate a constant oxygen condition which is assumed to be true during the initial phase of the autoxidation process. As Cloe is a gas phase solver, an elevated pressure is employed to simulate the equivalent concentration of the liquid phase at the desired temperature. The values are shown in Table 1. The fractional ratio of toluene and oxygen is assumed to be best described by the expected ratio at 298.15 K and 1.17×10^6 Pa, which results in an input of 98.79% of toluene and 1.21% of oxygen.

3.5. Summary of Models Considered. This study considers the development of an RMG model, which consists of a base model which is extended by the addition and inclusion of termination reactions of radical intermediates in the formation of the primary oxidation products. The resultant model is then subject to updates to the thermodynamic data of the initial species, small oxygenated products, as well as all primary oxidation products. The initial model consists of 118 species, excluding inert gases, and 2192 reactions. The termination reactions add 55 termination species, which involve every combination of possible R_2, R_2O, R_2O_2, R_2O_3, and R_2O_4 as well as the RO_3, which is the decomposition path for the R_2O_4 termination species.[73] These 54 species add 114 reactions to the mechanism. In the final step, the thermodynamic data of 32 key species, which cover the initial species, small oxygenated species, and all primary oxidation products are updated. The mechanism sizes are tabulated in Table 6, while an overview of the updated species was given previously in Table 2.

Table 6. Overview over the Sizes of the Employed Mechanisms

mechanism	number of	
	species	reactions
core mechanism	118	2192
extended mechanism	173	2309
improved mechanism	173	2309

4. RESULTS AND DISCUSSION

We begin with a brief presentation of the qualitative GC results obtained, shown in Section 4.1. Following, the overall behavior of the RMG mechanism is discussed in Section 4.2, focusing first on the core mechanism and the impact of termination reactions in the extended mechanism in Section 4.2.1 and then the impact of the updated quantum chemistry in the improved mechanism in Section 4.2.2. The impact of the oxygen concentration as a potential source of error in the comparison of the models is discussed in Section 4.3.

4.1. Qualitative Gas Chromatography Mass Spectrometry Analysis. In order to confirm that expected species from the literature are observed in the experiment, qualitative analysis of the samples was carried out using gas chromatography mass spectrometry. Pure, unstressed toluene, was analyzed to establish a reference composition relative to the stressed samples. It was found that only trace quantities of ethylbenzene are present as a contaminant, which explains its presence in the stressed sample. The chromatograms obtained with the PONA column for samples retrieved after a 10%, 20%, and 40% pressure drop at 160 °C are shown in Figure 2. A magnification of the time from 35 to 55 min is shown in Figure 3 to visualize the development of the peak intensity more clearly.

As can be seen from Figure 2, additional compounds are formed as a result of the thermal stress under a pressurized oxygen atmosphere, with their abundance increasing with an increased residence time, evidenced by the larger peaks for the 40% pressure drop criteria. Similarly, a higher stressing temperature corresponds to a greater amount of product formed. Benzoic acid was also only observed in the sample stressed at 160 °C. An identification of key peaks was carried out,[87−89] and a number of compounds were identified in agreement with the literature[2,90] shown in Table 7.

While an evaluation of the surface area of the gas chromatography mass spectrometry peaks for benzyl alcohol, benzaldehyde, and the cresol peaks cannot offer a robust quantification, it can offer preliminary data on the relative development of the species concentration in the sample. Values for the peak areas of the undiluted samples obtained with the PONA column are shown in Table 8. While benzyl alcohol exhibits a gradual concentration increase, the rate of production of benzaldehyde appears to accelerate. In contrast, the rate of cresol accumulation appears to be decreasing with increased oxidation. If we now take the reduced volume, relative to the initial 5 mL sample into account, we observe a consistent decrease in the total amount of the products observed. These increases in the surface area may be due to volume reduction, inducing a concentration of the oxidation products in the liquid phase. The limited number of data points focused on the liquid phase and suggests that further work which investigates the gas liquid exchange and equilibria is required.

4.2. Global Reactivity. *4.2.1. Core and Extended Mechanism Evaluation.* The induction periods relative to the experimental induction periods for the three model development stages is shown in Figure 4. An immediate observation that can be made is that the core mechanism, as generated by RMG without any modifications, is significantly too fast, which is to be expected, giving the missing termination reactions, which provide an essential sink for radical species. As shown in Figure 4, the addition and thus inclusion of termination reactions reduces the discrepancy between the experimental data and the model.

This is also evident in the ROP analysis, where consumption of toluene by the peroxyl radical at the induction period, the dominant path of toluene consumption, has been reduced by about a factor of 224 as a result of the addition of the termination reactions, shown in Table 9.

The oxidation inhibiting effect of the termination species further results in a more reasonable development of species concentrations over time when compared to the original mechanism. The addition of termination reactions has resulted in a more gradual consumption of the fuel, which agrees with
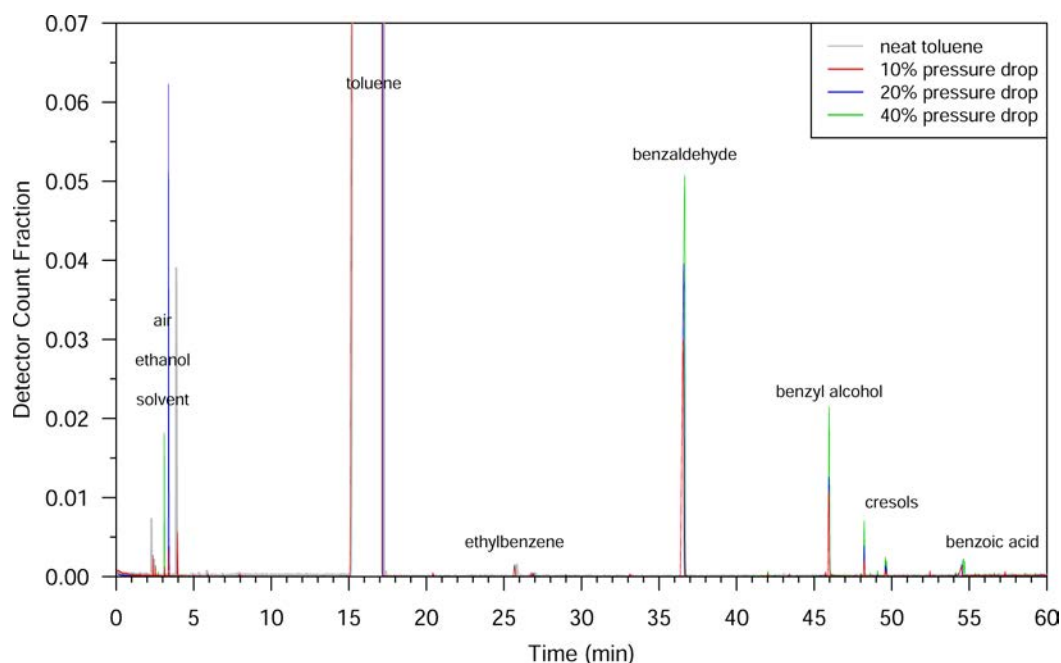
Figure 2. Chromatograms obtained using a PONA column in GC-MS, from a toluene sample subject to a 10%, 20%, and 40% pressure drop termination criteria at 160 °C in the PetroOxy. Neat toluene is shown in the background as a comparison.
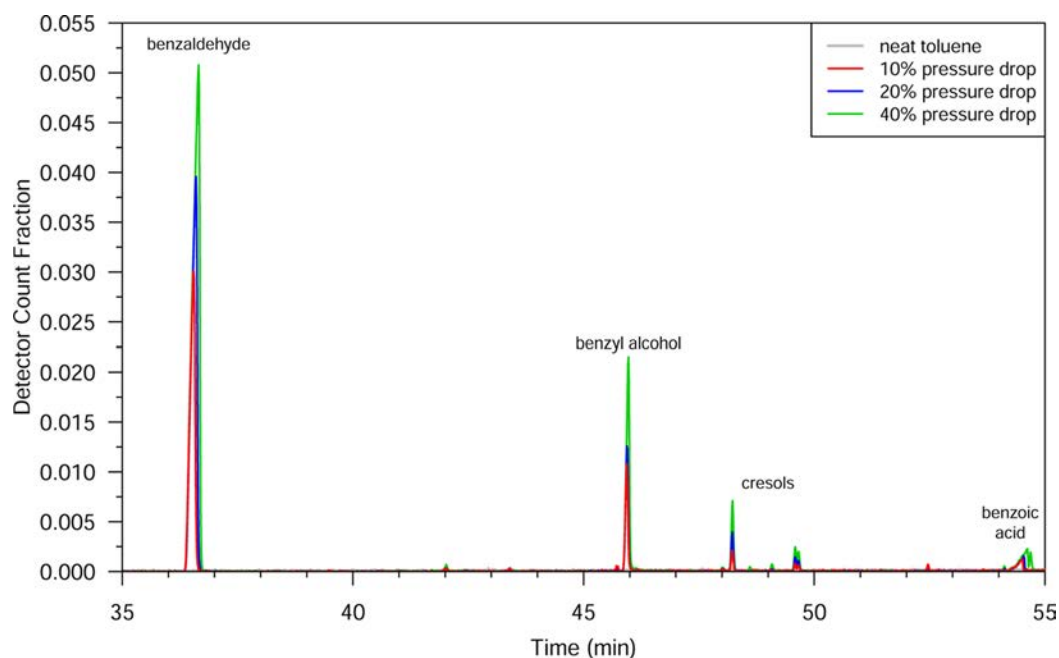
Figure 3. Focus on the 35 min to 55 min segment of the chromatograms, shown in Figure 2, obtained using a PONA column in GC-MS, from a toluene sample subject to a 10%, 20%, and 40% pressure drop termination criteria at 160 °C in the PetroOxy. Neat toluene is shown in the background as a comparison.

the literature as well as the gradual pressure drop, corresponding to a consumption of oxygen in the headspace by the fuel, observed in the experiment.

In agreement with the literature, the rate of production analysis applied to the core mechanism shows that a hydrogen abstraction by a peroxyl species dominates the toluene consumption in the mechanism, leading to the formation of a hydroperoxide and reactive alkyl, i.e., the reversible reaction R· + ROOH = RH + ROO· and not other reactions in the mechanism.[1,2,13,16] This is expected, as hydrogen abstraction by

oxygen is known to be slow, while peroxyl radicals are known to be highly reactive.[1,2,16,73] The mechanism strongly favors reactivity on the methyl group, shown in Table 9. Products such as benzyl alcohol, benzaldehyde, and benzoic acid are reported as being the dominant reaction route.[1,2] The resultant alkyl radical is then far more receptive to an interaction with any dissolved oxygen leading to another peroxyl species and thus propagating the reaction chain as has been previously reported for fuels.[13] Sensitivity analysis of the toluene species, filtered to include only reactions with a notable impact on the

Table 7. Species Identified in Samples from the PetroOxy with the Chromatogram Shown in Figure 2

time for peak (min)	species
2−4	air, ethanol, solvent
15−17	toluene
26	ethylbenzene
36	benzaldehyde
46	benzyl alcohol
48, 50	cresol
54−55	benzoic acid

mechanism, is shown in Supplementary Figure A.1 for the core and Supplementary Figure A.2 for the extended mechanism. As expected, the mechanism exhibits a large response to any modification of this reaction parameter (Reaction 19, see Table 9 for the identification of individual reactions). The reaction is discussed in more detail in Section 4.2.2, as its reaction equilibrium is impacted by the update to the thermodynamic data.

Another indicator with regard to the quality of the model aside from the induction period is the development of key species concentration profiles. The profile for the extended mechanism is shown in Figure 5. From a general qualitative point of view, the very low concentrations of both benzyl alcohol and benzaldehyde disagree with published observations that tend to report higher concentrations of products relative to toluene consumed, such as for example Hoorn et al.[1] In addition, the literature reports greater benzaldehyde concentrations than benzyl alcohol, a trend that is reversed in the extended mechanism. This is explained in the literature[1,91,92] by suggesting that a direct reaction path from toluene to both benzaldehyde and benzyl alcohol exists, after which the benzyl alcohol can be oxidized further to form benzaldehyde. Benzaldehyde is then only consumed in the formation of benzoic acid.

4.2.2. Improved Mechanism with Updated Thermodynamic Data Using Quantum Chemistry. The following step in the mechanism improvement consisted of the calculation of new thermodynamic parameters for all participating species up to the primary oxidation products, with the overview given previously in Table 2. Calculated values for the enthalpy of formation and entropy are given in Supplementary Table 5 and Table 6. As is immediately visible, the agreement of the mechanism with respect to the induction period at the higher temperature end at 140 °C (413.15 K) and 160 °C (433.15 K) has improved significantly, with the mechanism being maybe 0.2 orders of magnitude too slow with respect to the induction
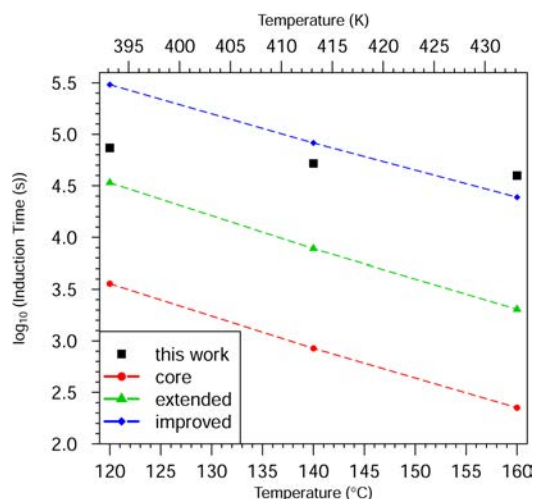
Figure 4. Plot of the logarithm of the induction time in seconds from the PetroOxy versus temperature, showing the core mechanism as well as the extended mechanism with added termination reactions and the improved mechanism with updated thermodynamic data using quantum chemistry calculations in ORCA.[76]

period in seconds at 140 °C (413.15 K) and 0.2 orders of magnitude too fast at 160 °C (433.15 K). Compared to the extended mechanism with added terminations, the consumption of toluene is roughly an order of magnitude slower, as shown previously in Table 9.

This can be explained by the observation that RMG writes certain reactions in a reverse format, such as the extremely sensitive reaction RH + ROO· → R· + ROOH, which is written as R· + ROOH ↔ RH + ROO·. The hydrogen abstraction from fuel by the peroxyl is reaction R19 in Figure 9. As this is a reverse reaction in the RMG generated reaction mechanism, the reverse rate constant is dependent on the thermodynamic parameters of the participating species and determined by the equilibrium constant. The calculation of Arrhenius parameters for the reverse reaction[93] reveals that the thermodynamic data from RMG result in a reaction that is between 0.5−0.75 orders of magnitude faster at low temperatures compared to the rate constants reported by Denisov.[73] Assuming Arrhenius behavior with no temperature dependence of the pre-exponential factor, $n = 0$, it is possible to fit an Arrhenius expression to the rate constants reported by Denisov[73] to estimate suitable reference values in the narrow 298.15−433.15 K temperature range, with the fitted values for A and E_a shown in Table 10. The corresponding plot of k versus T is shown in Figure 6. When the thermodynamic parameters for the species in the reaction

Table 8. Peak Areas for the Chromatogram Obtained with a PONA Column for a Sample Stressed at 160 °C

	undiluted sample			considering volume loss	
compound	peak at 10%	peak at 20%	peak at 40%	at 20%	at 40%
benzyl alcohol	1.01×10^9	1.53×10^9	2.33×10^9		
relative to 10%		+52%	+131%	−34%	−56%
relative to 20%			+52%		−34%
benzaldehyde	1.86×10^8	2.26×10^8	4.25×10^8		
relative to 10%		+22%	+129%	−18%	−56%
relative to 20%			+88%		−47%
cresols (combined)	4.80×10^7	8.94×10^7	1.58×10^8		
relative to 10%		+86%	+129%	−46%	−40%
relative to 20%			+77%		−43%

Table 9. Overview of the Most Important Reactions Involved in the Consumption of Toluene at the Time of the Induction Period in the Mechanism, for the 433.15 K Temperature Criteria, Presented as Rate of Production and Sorted by Rate for the Improved RMG Mechanism

reaction number	reaction	core mechanism		extended mechanism		improved mechanism	
		fraction	mol cm^{-3} s^{-1}	fraction	mol cm^{-3} s^{-1}	fraction	mol cm^{-3} s^{-1}
9	$C_7H_7(7)$ + oxygen(2) $\leftrightarrow$ $C_7H_7O_2(11)$	−0.982	−4.95 × 10^{-4}	−0.965	−2.24 × 10^{-6}	−0.609	−1.68 × 10^{-7}
79	oxygen(2) + $C_7H_5O(44)$ $\leftrightarrow$ $C_7H_5O_3(64)$	−0.018	−8.84 × 10^{-6}	−0.032	−7.40 × 10^{-8}	−0.357	−9.87 × 10^{-8}
367	oxygen(2) + $C_7H_7O(19)$ $\leftrightarrow$ HOOJ(5) + $C_7H_6O(43)$	0	−1.65 × 10^{-9}	−0.002	−4.93 × 10^{-9}	−0.011	−3.04 × 10^{-9}
15	$C_7H_7(9)$ + oxygen(2) $\leftrightarrow$ $C_7H_7O_2(13)$	0	−4.19 × 10^{-8}	0	−3.49 × 10^{-10}	−0.004	−1.03 × 10^{-9}
14	$C_7H_7(8)$ + oxygen(2) $\leftrightarrow$ $C_7H_7O_2(12)$	0	−4.19 × 10^{-8}	0	−3.49 × 10^{-10}	−0.004	−1.02 × 10^{-9}
85	oxygen(2) + $C_7H_7O(58)$ $\leftrightarrow$ $C_7H_7O_3(73)$	0	−1.08 × 10^{-8}	0	−9.71 × 10^{-11}	−0.004	−1.02 × 10^{-9}
78	oxygen(2) + $C_7H_7O(57)$ $\leftrightarrow$ $C_7H_7O_3(60)$	0	−1.05 × 10^{-8}	0	−9.44 × 10^{-11}	−0.004	−1.00 × 10^{-9}
16	$C_7H_7(10)$ + oxygen(2) $\leftrightarrow$ $C_7H_7O_2(14)$	0	−2.10 × 10^{-8}	0	−1.74 × 10^{-10}	−0.002	−5.12 × 10^{-10}
86	oxygen(2) + $C_7H_7O(59)$ $\leftrightarrow$ $C_7H_7O_3(76)$	0	−5.11 × 10^{-9}	0	−4.61 × 10^{-11}	−0.002	−5.10 × 10^{-10}
43	oxygen(2) + $C_7H_7O_2(28)$ $\leftrightarrow$ $C_7H_7O_4(32)$	0	−3.09 × 10^{-8}	0	−2.54 × 10^{-10}	−0.002	−4.24 × 10^{-10}
42	oxygen(2) + $C_7H_7O_2(27)$ $\leftrightarrow$ $C_7H_7O_4(31)$	0	−3.09 × 10^{-8}	0	−2.54 × 10^{-10}	−0.002	−4.22 × 10^{-10}
44	oxygen(2) + $C_7H_7O_2(29)$ $\leftrightarrow$ $C_7H_7O_4(33)$	0	−1.54 × 10^{-8}	0	−1.27 × 10^{-10}	−0.001	−2.12 × 10^{-10}
69	oxygen(2) + $C_7H_5O(45)$ $\leftrightarrow$ $C_7H_5O_3(48)$	0	−4.49 × 10^{-12}	0	−6.94 × 10^{-14}	0	−4.00 × 10^{-11}
70	oxygen(2) + $C_7H_5O(46)$ $\leftrightarrow$ $C_7H_5O_3(49)$	0	−4.49 × 10^{-12}	0	−6.94 × 10^{-14}	0	−4.00 × 10^{-11}
71	oxygen(2) + $C_7H_5O(47)$ $\leftrightarrow$ $C_7H_5O_3(50)$	0	−2.25 × 10^{-12}	0	−3.47 × 10^{-14}	0	−2.07 × 10^{-11}
374	HOOJ(5) + $C_7H_7O(22)$ $\leftrightarrow$ oxygen(2) + $C_7H_8O(26)$	0	3.58 × 10^{-14}	0	1.55 × 10^{-13}	0	1.44 × 10^{-12}
378	HOOJ(5) + $C_7H_7O_3(37)$ $\leftrightarrow$ oxygen(2) + $C_7H_8O_3(40)$	0	5.30 × 10^{-14}	0	2.27 × 10^{-13}	0	2.70 × 10^{-12}
380	HOOJ(5) + $C_7H_7O_3(38)$ $\leftrightarrow$ oxygen(2) + $C_7H_8O_3(41)$	0	5.40 × 10^{-14}	0	2.28 × 10^{-13}	0.001	4.69 × 10^{-12}
383	HOOJ(5) + $C_7H_7O_3(76)$ $\leftrightarrow$ oxygen(2) + $C_7H_8O_3(42)$	0	1.79 × 10^{-14}	0	8.32 × 10^{-14}	0.002	1.03 × 10^{-11}
358	2HOOJ(5) $\leftrightarrow$ HOOH(6) + oxygen(2)	0	4.25 × 10^{-18}	0	1.15 × 10^{-12}	0.003	1.52 × 10^{-11}
379	HOOJ(5) + $C_7H_7O_3(60)$ $\leftrightarrow$ oxygen(2) + $C_7H_8O_3(40)$	0	3.61 × 10^{-14}	0	1.68 × 10^{-13}	0.003	1.90 × 10^{-11}
381	HOOJ(5) + $C_7H_7O_3(73)$ $\leftrightarrow$ oxygen(2) + $C_7H_8O_3(41)$	0	3.56 × 10^{-14}	0	1.66 × 10^{-13}	0.003	2.01 × 10^{-11}
394	HOOJ(5) + $C_7H_5O_3(64)$ $\leftrightarrow$ oxygen(2) + $C_7H_6O_3(65)$	0.002	3.29 × 10^{-12}	0.002	1.44 × 10^{-11}	0.017	1.03 × 10^{-10}
363	HOOJ(5) + $C_7H_7O_2(11)$ $\leftrightarrow$ oxygen(2) + $C_7H_8O_2(15)$	0.998	1.65 × 10^{-9}	0.642	3.86 × 10^{-9}	0.417	2.48 × 10^{-9}
2195	$C_7H_7O(19)$ + oxygen(2) $\leftrightarrow$ S(116)			0.355	2.13 × 10^{-9}	0.552	3.28 × 10^{-9}
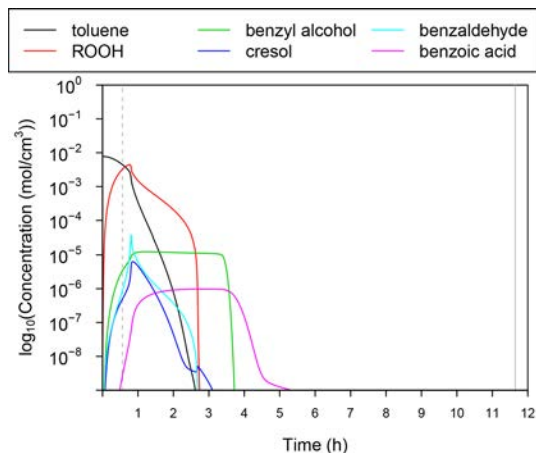
Figure 5. Concentrations profile for key species in the RMG model with added termination reactions at 433.15 K.

Table 10. Arrhenius Parameters for Reaction R· + ROOH = RH + ROO· in the Liquid Phase, Forward as Estimated by RMG and Reverse, Calculated from the Original RMG-Py Thermochemistry and the Updated ORCA[76] Thermochemistry[a]

R· + ROOH = RH + ROO·	A (mol cm^{-3} s^{-1})	n	E_a (kcal/mol)
forward	2.959 × 10^{-3}	4.241	5.004
RMG-Py thermo reverse	4.127 × 10^{-12}	6.889	3.378
ORCA thermo reverse	3.003 × 10^{-6}	5.172	7.036
Denisov k reverse fitted	9.3 × 10^{9}	0	10.523

[a]Values fitted to Denisov's[73] rate constant for the reverse reaction for comparison purposes.

mechanism are recalculated using quantum chemistry, we observe that the calculated reverse rate constant closely agrees with the data reported by Denisov,[73] shown in Figure 6, and reproduces the temperature dependence of the fitted parameters well over a narrow 150 K temperature range.

The individual contributions of the species whose thermodynamic data was updated go beyond the single reaction discussed here. The overall impact is a significant reduction of the reactivity leading to a better agreement of the model with experimental data with regard to the induction period as can be seen in Figure 4. The difference in the predicted induction period at the low temperature improved from being around three-quarter orders of magnitude too fast with the added terminations, to be around a tenth of an order of magnitude too fast with the updated thermodynamic data. Unfortunately, the updates to the thermodynamic data did not resolve the temperature dependence of the model. At the low temperature of 120 °C (393.15 K), the model is around 0.6 orders of magnitude too slow, while now in good agreement at the intermediate temperature of 140 °C (413.15 K). It remains too fast at the high temperature of 160 °C (433.15 K) by about 0.2 orders of magnitude.

The update of the thermodynamic data has led to a significant improvement with respect to the induction period. However, close scrutiny of the species concentration development reveals that benzoic acid is no longer formed in the mechanism. The rate of production analysis reveals that this is
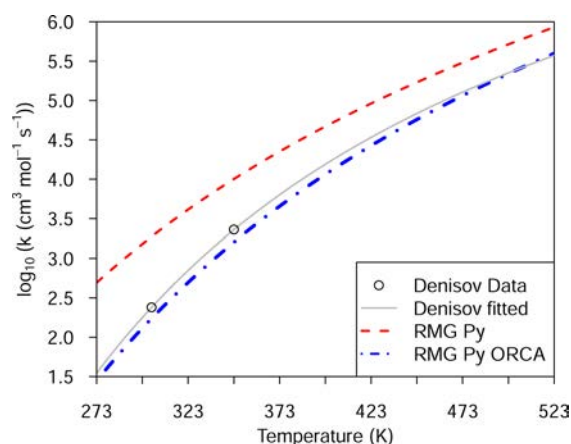
Figure 6. Plot of rate constants k in $cm^3\ mol^{-1}\ s^{-1}$, value from RMG-Py as generated, resulting value after updating the thermodynamic parameters of participating species as well as the value fitted to Denisov's data[73] when $n = 0$ is assumed.

the result of the benzoyloxyl radical decomposing only into a phenyl radical and stable carbon dioxide molecule, as shown in Figure 7. Prior to the update of the thermodynamic data, the
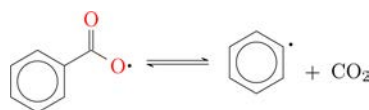
Figure 7. Illustration of the bezoyloxy radical decomposition reaction which is badly estimated in the RMG mechanism.

mechanism exhibited a split distribution of the benzoyloxyl radical consumption, with roughly half of the benzoyloxyl radicals dissociating and the other half abstracting a hydrogen from toluene to form benzoic acid.

The related decomposition of benzoyl peroxide is the closest related reaction discussed in the literature.[94−96] While the dissociation of the bezoyloxy radical is mentioned as a part of the decomposition mechanism,[95,96] the primary focus lies with

the decomposition of bezoyl peroxide.[95,97,98] Hence these studies can only offer a preliminary indication with respect to the expected rate constant.

One of the simplest parameters to assess in this reaction is the activation energy associated with the dissociation of CO_2 to form a phenyl molecule. To this effect, a relaxed potential energy surface scan with multiplicities of both two and four was carried out using M06-2X, ωB97X-D3, as well as RI-B2PLYP, chosen for their good performance, with a def2-TZVP basis set.[53,68] During the scan it can be observed that the functional "breaks down" providing inaccurate energy predictions with a multiplicity of two. This corresponds to the change from a linear to a bent CO_2 molecule. Most likely a triple-radical briefly forms as a transition state, in which a C=O bond is broken to form a single C−O bond and a biradical, with a radical electron each on the carbon and oxygen. This would then allow the carbon radical electron to interact with the phenyl radical electron to form a bond between the two species. In reverse, when the bond is broken, the radical electron of the carbon will need to interact with the radical electron on the oxygen first, before the CO_2 molecule obtains its expected linearity. In contrast to a calculation carried out with a multiplicity of two, the calculation carried out with a multiplicity of four results in a smooth overlapping plot of energy versus bond length. The authors suggest that future work should use multireference methods which are able to capture such behavior adequately; however, these are beyond the scope of this work.

The primary aim of the calculation was to establish reasonable limits for the activation energy associated with the dissociation of CO_2 from $C_7H_5O_2$. For small acids, such as acetic acid, an activation energy of the order of around 60 kcal·mol^{-1} is reported.[99] RMG does also predict the decomposition of benzoic acid, forming benzene and carbon dioxide, with an activation energy of around 75 kcal·mol^{-1}. However, for the decomposition of the $C_7H_5O_2$ radical, no data could be found. The decomposition of benzoyl peroxide is a related field and offers some limited data;[94,95] however, as the kinetics are dominated by the breaking of the peroxide bond, it can only
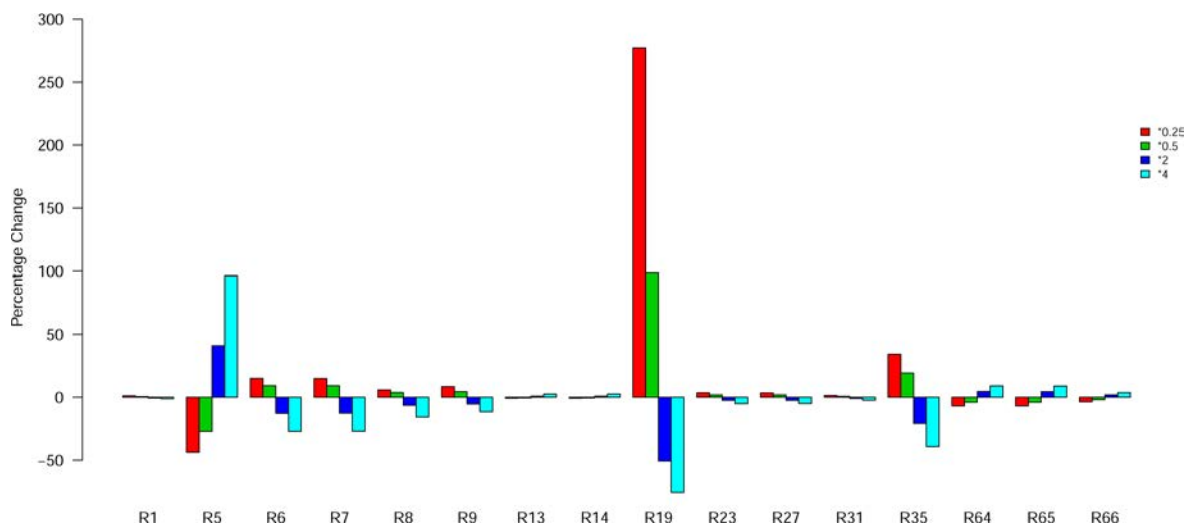
Figure 8. Sensitivity analysis carried out on the A parameter for all reactions involving toluene, in the final mechanism with updated thermodynamic parameters, assessing the impact of a modification on the induction period at 160 °C (433.15K). A was multiplied with 0.25, 0.5, 2, and 4, with the reported change relative to the unmodified mechanism. The intermediate mechanisms are shown in Supplementary Figure A.1 and Figure A.2. The reaction key is provided in Figure 9.

provide a lower limit for the expected rate. Carrying out the scan calculation suggests that the activation energy most likely lies in the range of 10−13 kcal/mol (≈40−60 kJ/mol), higher than the RMG-predicted activation energy of 6.13 kcal/mol (25.6 kJ/mol), but well below the activation energy required for the decomposition of acids.

In lieu of better data we have therefore decided to employ an activation energy of 10 kcal·mol^{-1} in the mechanism, while fitting both A and n to the published rate constants, which present a lower limit.[95] The resultant mechanism then again shows a production of benzoic acid, as is observed experimentally, both in this work and the literature.[1,2,90] Assessing the impact of the reaction rate on concentrations, sensitivity analysis was carried out, varying A by factors from 1 × 10^{-3} to 1 × 10^{10} showed no visible difference in concentration profiles in the model. Nevertheless, it is recommended that future work should seek to employ a more robust theoretical methodology if no experimental data for suitable reaction parameters may be obtained.

The application of sensitivity analysis to the toluene consumption indicates that the high sensitivity to the hydrogen abstraction from toluene by the peroxyl radical, as shown in Figure 8, with a level similar to the sensitivity exhibited in the extended mechanism with added termination reactions. Sensitivity analysis applied to the Arrhenius parameters, A, n, and E_a suggests that the mechanism remains insensitive with respect to the temperature dependence of the mechanism when investigating reactions involving toluene, the peroxyl radical ROO, as well as the termination reactions. The result of sensitivity analysis applied to the A parameter for reactions involving toluene is shown in Figure 10. As can be seen, the

R1	toluene(1) + oxygen(2)=HOOJ(5) + C7H7(7)
R5	toluene(1) + HOJ(3)=H2O(4) + C7H7(7)
R6	toluene(1) + HOJ(3)=H2O(4) + C7H7(8)
R7	toluene(1) + HOJ(3)=H2O(4) + C7H7(9)
R8	toluene(1) + HOJ(3)=H2O(4) + C7H7(10)
R9	toluene(1) + HOOJ(5)=HOOH(6) + C7H7(7)
R13	toluene(1) + C7H7(8)=toluene(1) + C7H7(7)
R14	toluene(1) + C7H7(9)=toluene(1) + C7H7(7)
R15	toluene(1) + C7H7(10)=toluene(1) + C7H7(7)
R19	C7H7(7) + C7H8O2(15)=toluene(1) + C7H7O2(11)
R23	C7H8O2(16) + C7H7(7)=toluene(1) + C7H7O2(12)
R27	C7H7(7) + C7H8O2(17)=toluene(1) + C7H7O2(13)
R31	C7H7(7) + C7H8O2(18)=toluene(1) + C7H7O2(14)
R35	toluene(1) + C7H8O(19)=C7H7(7) + C7H8O(23)
R36	C7H7(8) + C7H8O(23)=toluene(1) + C7H7O(19)
R64	C7H7(8) + C7H8O2(15)=toluene(1) + C7H7O2(30)
R65	C7H7(9) + C7H8O2(15)=toluene(1) + C7H7O2(30)
R66	C7H7(10) + C7H8O2(15)=toluene(1) + C7H7O2(30)

Figure 9. List of reactions displayed in the sensitivity analysis in Figure 8 and Supplementary Figures A.1 and A.2.

largest change in the temperature dependence was on the order of about 1 × 10^{-3} s, where at least approximately 2 × 10^{-2} s would be required to reduce the slope over the temperature range of 40 K corresponding to our experimental data. This is the same behavior as exhibited by both the core and extended mechanism, for which the A parameter sensitivity is shown in Supplementary Figures A.3 and A.4.

This suggests that there may be a reaction path which is not captured by the current model which influences the balance of species in the model and thus would reduce the currently observed error in the temperature dependency. As the mechanism's behavior is dominated by the reactions of the peroxyl radical, some kind of radical sink which increases reactivity with temperature would be the obvious choice.

However, while termination reactions would seem to be good candidates, their reactivity has been shown to decrease with temperature.[100] Alternatively it is possible that RMG does not capture the effects of reactivity-inhibiting species properly, as the toluene conversion has been reported to decrease with an increase in products of certain species, such as cresols.[2] In contrast, toluene conversion in the RMG generated model does not decrease, but after an acceleration phase, continues until the fuel has been fully consumed. Another possibility is that updates to some of the secondary oxidation products may change the mechanism's behavior, despite these not featuring prominently in the reactions of the current mechanism.

One example of a reaction not considered by RMG would be the Bayer−Villiger reaction which offers another reaction path to benzoic acid. It has been discussed theoretically;[1,73] however, no Arrhenius parameters or rate constants are given, precluding its manual inclusion into the mechanism. In addition there may be other "side channel reactions" in which species participate that have not been considered by RMG, which would change the reactivity of the mechanism.

Further insight into the quality of the model can be obtained from a qualitative assessment of the concentration development of the model. The core and extended mechanism with RMG-calculated thermodynamic data was previously discussed with the results shown in Figure 5. The concentration development for the improved RMG mechanism with updated thermodynamic parameters is shown in Figure 11. Immediately visible improvements in the mechanism are the larger concentration of benzaldehyde when compared to benzyl alcohol as well as the relative stability of species over time.[1,2]

A quantitative comparison with literature data is unfortunately not possible as despite broadly similar experimental setups the observed behavior was significantly different. In the more recent study, Hermans et al.[2] oxidized 50 mL of toluene in a stirred 100 mL high pressure Parr reactor at 433 K, which was initially pressurized to 2.67 MPa with oxygen under standard temperature conditions. The reported stirring of the sample at 500 rpm was employed to ensure that the experiment was not diffusion limited.[2] Toluene conversion as a function of time is reported by Hermans et al.[2] and reaches roughly 0.3% at 2 h. A maximum conversion of approximately 4% is reported after 12 h. While the work is not directly comparable, a data point for Hermans' toluene conversion is shown in Supplementary Figure A.7, where the data point from Hermans et al.[2] refers to a 4% fuel consumption. The higher oxygen pressure employed by Hermans et al.[2] would not result in any difference in the model behavior, as is shown in Section 4.3, where the impact of the oxygen concentration on the model is discussed.

The older study by Hoorn et al.[1] was carried out under temperatures from 423 to 433 K in a 250 mL Parr autoclave, operated under 7 × 10^5 Pa of pressure, which was also stirred during the experiment. However, instead of an initial pressurization, oxygen is continuously bubbled through the sample. In this setup, Hoorn et al.[1] report a constant consumption rate of toluene, which sees the concentration of toluene drop by roughly 30% in 2 h. The toluene consumption is not measured directly but calculated from the production of benzoic acid, the dominant product with a maximum fraction by weight of around 30% and the trace quantities of benzaldehyde and benzyl alcohol which have maximum fractions of roughly 2.5% and 1.6%.
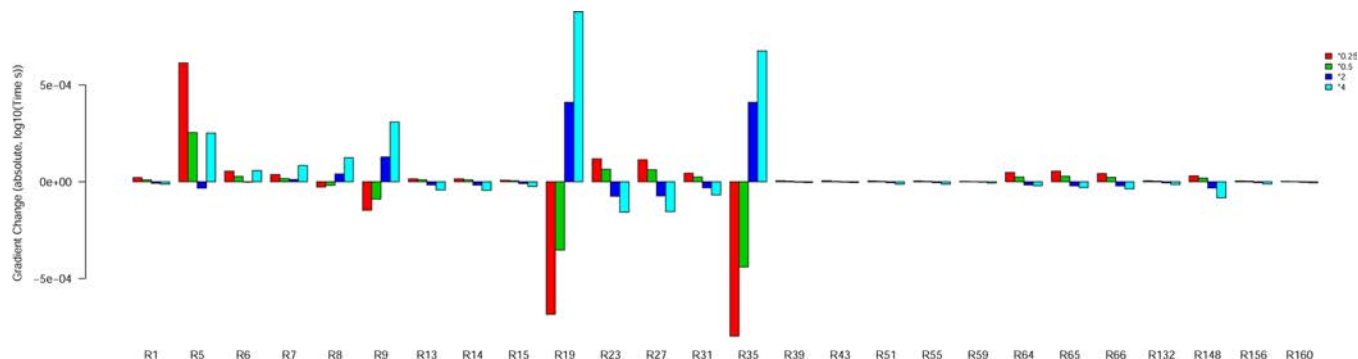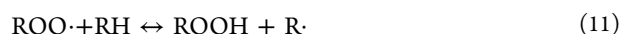
Figure 10. Sensitivity analysis applied to the mechanism with updated thermodynamic parameters on the *A* parameter for all reactions involving toluene, assessing the impact on the temperature dependence of the mechanism. *A* was multiplied with 0.25, 0.5, 2, and 4, with the reported change relative to the unmodified mechanism. The reaction key is provided in Figure 9. See Supplementary Figure A.3 and Figure A.4 for the intermediate schemes.
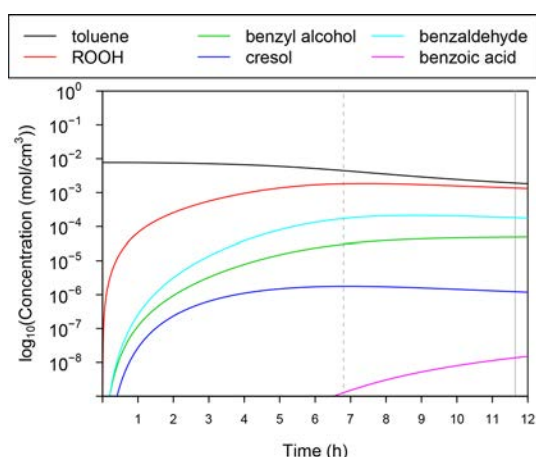
Figure 11. Concentrations profile for key species in the RMG model with added termination reactions and updated thermodynamic data at 433.15 K. The experimental induction period is indicated by a solid gray line, while the model induction period is indicated by a dashed gray line.

While a quantitative comparison with the experimental data by Hermans et al.[2] is not possible, it is possible to comment qualitatively on the performance of the mechanism in comparison with the literature. In agreement with Hermans et al.[2] and Hoorn,[1] the toluene autoxidation mechanism follows the standard outline of hydrocarbon autoxidation. Initially, a hydroperoxide species is formed on the methyl group which then reacts further to form both benzyl alcohol and benzaldehyde. These can then be oxidized further to produce benzoic acid as the final species in the oxidation process. In addition, cresols, discussed by Hermans et al.,[2] are also considered in the presented mechanism, as well as relevant peroxyl, oxyl, and hydroperoxide precursor species in the formation of said cresols. For the sake of simplicity, reactions are detailed on the methyl group only, which is the dominant reaction pathway. Both Hermans et al.[2] and the RMG mechanism follow the standardized autoxidation mechanism as shown in the following eqs 10, 11, 12, 13, and 14. A key with the structures drawn out for every named species is shown in Supplementary Table 4.

$$R \cdot + O_2 \leftrightarrow ROO \cdot \qquad (10)$$

$$ROO \cdot + RH \leftrightarrow ROOH + R \cdot \qquad (11)$$

$$ROOH \leftrightarrow RO \cdot + HO \cdot \qquad (12)$$

$$H_2O_2 + ROO \cdot \leftrightarrow HO_2 \cdot + ROOH \qquad (13)$$

$$HO_2 \cdot + RH \leftrightarrow H_2O_2 + R \cdot \qquad (14)$$

Reactions that are inherently not considered by RMG include trimolecular reactions, nonfundamental reactions, as well as cage reactions, the latter which are discussed extensively by Hermans et al.[2] Looking further at the reactions involving benzyl alcohol and benzaldehyde, the mechanisms between Hermans et al.[2] and RMG appear to diverge, at least when considering rate of production values at one induction period. While Hermans et al.[2] discuss the reactivity of benzaldehyde and benzyl alcohol in the context of larger species, such as a benzyl derived peroxyl, the RMG mechanism is instead centered around the "small species" such as the hydroxyl and peroxyl radical. However, this may be the result of the RMG mechanism being investigated under conditions in which oxygen is present in a constant concentration, which favors the presence of small oxygenated species. The RMG mechanism contains a large number of rearrangement reactions, as well as decomposition reactions discussed by Hermans et al.[2] such as reactions 15 and 16.

$$ROO \cdot \leftrightarrow Q \cdot OOH \qquad (15)$$

$$HO \cdot + R = O \leftrightarrow Q \cdot OOH \qquad (16)$$

In addition, in agreement with both Hermans et al.[2] and Hoorn,[1] precursors in the formation of benzoic acid are present in the presented mechanism, leading to its formation by reactions 17, 18, 19, and 20.

$$O_2 + R \cdot = O \leftrightarrow R(=O)OO \cdot \qquad (17)$$

$$R(=O)OO \cdot + RH \leftrightarrow R(=O)OOH + R \cdot \qquad (18)$$

$$R(=O)OOH \leftrightarrow R(=O)O \cdot + HO \cdot \qquad (19)$$

$$R(=O)O \cdot + RH \leftrightarrow R(=O)OH + R \cdot \qquad (20)$$
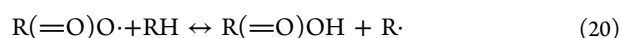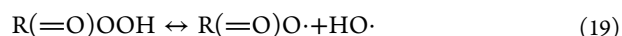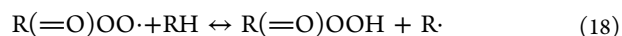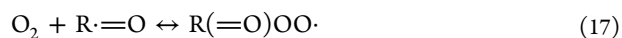
Alternatively, the improved mechanism also suggests the direct routes involving both the peroxyl radical and the hydroxyl radicals, shown in reactions 21 and 22, where the perbenzoic acid from reaction 20 can then continue the reactions steps from reaction 19 to form benzoic acid.[6]

$$HO_2 \cdot + R \cdot = O \leftrightarrow R(=O)OOH \qquad (21)$$

$$HO + R\cdot = O \leftrightarrow R(= O)OH \tag{22}$$
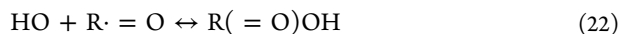
The cresols and intermediate radical species follow the same established general autoxidation chemistry in both the paper by Hermans et al.[2] as well as the RMG mechanism. While both Hermans et al.[2] and Hoorn[1] suggest that two benzyl-peroxyls will terminate with the formation of benzyl alcohol, benzaldehyde, and oxygen, RMG favors the pathway suggested by Denisov.[73] This is outlined in reactions 23, 24, and 25. Instead of benzaldehyde, these steps lead to the formation of a benzyl-oxyl radical, RO·, which can form benzyl alcohol by hydrogen abstraction from the main fuel or another species.

$$ROO\cdot + ROO\cdot \rightarrow ROO - OOR \tag{23}$$

$$ROO\text{-}OOR \rightarrow RO_3\cdot + RO\cdot \tag{24}$$

$$RO_3\cdot \rightarrow RO\cdot + O_2 \tag{25}$$

In this work, experimental data were collected in the PetroOxy using the method outlined in Section 2.1. The stressed sample was retained for a 10%, 20%, and 40% pressure drop condition. A comparison plot for the concentration of toluene in the experiment and the model is shown in Figure 12,
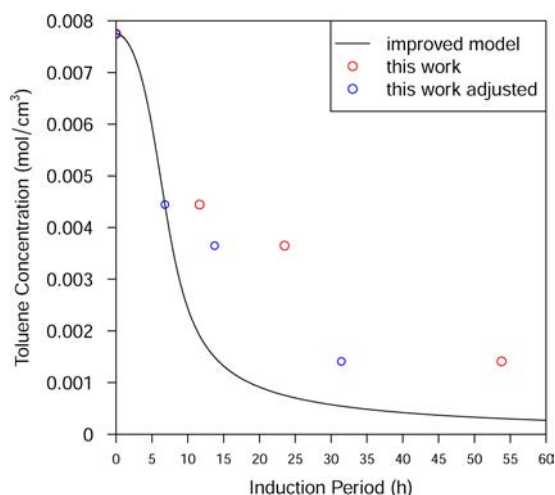
Figure 12. Comparison of model concentrations with experimentally obtained concentrations from a PetroOxy. The adjusted data points show the experimentally obtained values with a 58.4% offset in time, relative to the obtained experimental data, to account for the faster oxidation of the model observed for the 10% pressure drop criteria.

using the model concentration at 0 s as a 100% reference concentration. Both benzaldehyde and benzyl alcohol were qualitatively identified as oxidation products, in agreement with published literature.[1,2] Quantitative analysis of these species will be the subject of future work. As can be seen from the experimental data, the observed toluene consumption appears to follow a linear profile, which is also reflected in the observed pressure drop during the PetroOxy experiment. The model also exhibits a linear section; however, the reactivity is significantly higher, suggesting that some inhibiting effect is not yet properly incorporated into the model.

4.3. Oxygen Level Sensitivity. The nature of the sealed test chamber in the PetroOxy during the oxidation test results in an uncertainty with respect to the actual oxygen concentration in the fuel sample during the test, especially once the sample is heated, as the temperature of the solvent affects the solubility of gases in a solvent.[101] We made the

simplifying assumption that the expected oxygen concentration at the test pressure and test temperature is described accurately by applying Henry's Law to the case of a test pressure of 1.17×10^6 Pa using the oxygen solubility data for 298.15 K, assuming no temperature dependence,[73,74] which results in an oxygen concentration of 0.1024 mol/L. While the solubility of gases decreases with temperature for many solvents, recent experimental work suggests that the impact of temperature on the concentration of dissolved oxygen is small in the case of toluene,[102] which supports the use of the standard temperature for the calculations of the oxygen and fuel fractions during the test. As shown in Figure 13, the final model with termination
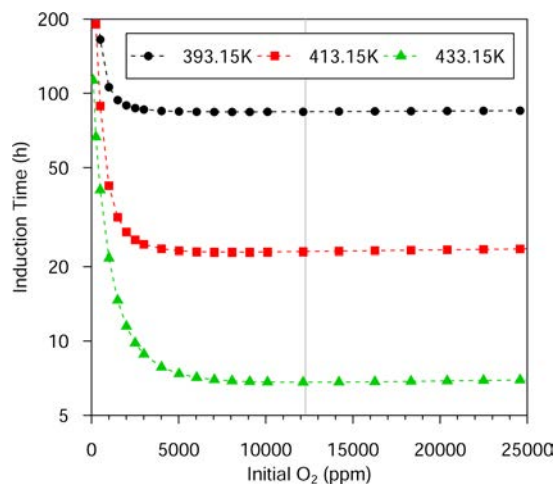
Figure 13. Impact of the initial oxygen concentration on the simulated induction period. The value calculated using Henry's Law and employed in this work is indicated by a gray line. Plot shown is for the final mechanism, intermediate mechanisms are shown in Supplementary Figure A.5 and Figure A.6.

reactions exhibits no large sensitivity to the oxygen concentration from about 2500 ppm of dissolved oxygen. The impact of the oxygen concentration for the core mechanism and extended mechanism is shown in Supplementary Figures A.5 and A.6. This suggests that the mechanism in its current form contains a rate limiting step with a threshold oxygen concentration of approximately 2500 ppm, beyond which the presence of additional oxygen will not accelerate the oxidation process. This is further beneficial as it reduces any error introduced from the uncertainty about the oxygen concentration in solution during the collection of experimental induction period data with the PetroOxy. At the same time, the model's response to the oxygen concentration suggests that reactivity decreases drastically at low concentrations corresponding to real life fuel applications. Oxygen consumption is dominated by an interaction with the benzyl radical to form a peroxyl radical. Said peroxyl radical is the dominant route for the conversion of toluene to the benzyl radical, formed by hydrogen abstraction from the fuel. This is shown at the time when the induction period is reached for every model in Table 11 and Table 12.

The same type of behavior can be identified in a previously published mechanism for octane autoxidation by Chatelain et al.;[16] however contrary to toluene, the effect is only observed at very low oxygen concentrations, significantly lower than in toluene, as shown in Supplementary Figure A.8. This can be explained by the fact that octane offers a larger number of

15

Table 11. Dominant Reactions in the Rate of Production of Oxygen at the Time of the Induction Period in the Mechanism, for the 433.15 K Temperature Criteria, Sorted by Rate for the Improved RMG Mechanism

reaction number	reaction	core mechanism		extended mechanism		improved mechanism	
		fraction	mol cm^{-3}·s^{-1}	fraction	mol cm^{-3}·s^{-1}	fraction	mol cm^{-3}·s^{-1}
137	$C_7H_7(7) + C_7H_8O_2(15) \leftrightarrow$ toluene(1) + $C_7H_7O_2(11)$	−0.993	−4.93 × 10^{-4}	−0.986	−2.22 × 10^{-6}	−0.664	−1.18 × 10^{-7}
123	toluene(1) + HOJ(3) ↔ $H_2O(4)$ + $C_7H_7(7)$	−0.005	−2.29 × 10^{-6}	−0.008	−1.89 × 10^{-8}	−0.22	−3.91 × 10^{-8}
266	toluene(1) + $C_7H_5O_3(64)$ ↔ $C_7H_7(7)$ + $C_7H_6O_3(65)$	−0.001	−2.49 × 10^{-7}	−0.001	−2.10 × 10^{-9}	−0.023	−4.11 × 10^{-9}
124	toluene(1) + HOJ(3) ↔ $H_2O(4)$ + $C_7H_7(8)$	0	−2.06 × 10^{-7}	−0.001	−1.70 × 10^{-9}	−0.02	−3.52 × 10^{-9}
125	toluene(1) + HOJ(3) ↔ $H_2O(4)$ + $C_7H_7(9)$	0	−2.06 × 10^{-7}	−0.001	−1.70 × 10^{-9}	−0.02	−3.52 × 10^{-9}
153	toluene(1) + $C_7H_7O(19)$ ↔ $C_7H_7(7)$ + $C_7H_8O(23)$	0	−1.35 × 10^{-9}	−0.002	−4.06 × 10^{-9}	−0.015	−2.74 × 10^{-9}
126	toluene(1) + HOJ(3) ↔ $H_2O(4)$ + $C_7H_7(10)$	0	−1.03 × 10^{-7}	0	−8.52 × 10^{-10}	−0.01	−1.76 × 10^{-9}
274	$C_7H_7(7) + C_7H_8O_3(41) \leftrightarrow$ toluene(1) + $C_7H_7O_3(73)$	0	−1.09 × 10^{-8}	0	−9.76 × 10^{-11}	−0.004	−7.88 × 10^{-10}
250	$C_7H_7(7) + C_7H_8O_3(40) \leftrightarrow$ toluene(1) + $C_7H_7O_3(60)$	0	−1.08 × 10^{-8}	0	−9.64 × 10^{-11}	−0.004	−7.26 × 10^{-10}
127	toluene(1) + HOOJ(5) ↔ HOOH(6) + $C_7H_7(7)$	0	−3.23 × 10^{-13}	0	−1.67 × 10^{-10}	−0.003	−6.09 × 10^{-10}
157	$C_7H_7(7) + C_7H_8O(24) \leftrightarrow$ toluene(1) + $C_7H_7O(20)$	0	−4.11 × 10^{-8}	0	−3.38 × 10^{-10}	−0.003	−5.29 × 10^{-10}
161	$C_7H_7(7) + C_7H_8O(25) \leftrightarrow$ toluene(1) + $C_7H_7O(21)$	0	−4.11 × 10^{-8}	0	−3.37 × 10^{-10}	−0.003	−5.17 × 10^{-10}
278	$C_7H_7(7) + C_7H_8O_3(42) \leftrightarrow$ toluene(1) + $C_7H_7O_3(76)$	0	−5.33 × 10^{-9}	0	−4.77 × 10^{-11}	−0.002	−3.94 × 10^{-10}
201	$C_7H_7(7) + C_7H_8O_3(41) \leftrightarrow$ toluene(1) + $C_7H_7O_3(38)$	0	−3.03 × 10^{-8}	0	−2.46 × 10^{-10}	−0.002	−3.38 × 10^{-10}
165	$C_7H_7(7) + C_7H_8O(26) \leftrightarrow$ toluene(1) + $C_7H_7O(22)$	0	−2.09 × 10^{-8}	0	−1.74 × 10^{-10}	−0.001	−2.33 × 10^{-10}
197	$C_7H_7(7) + C_7H_8O_3(40) \leftrightarrow$ toluene(1) + $C_7H_7O_3(37)$	0	−3.08 × 10^{-8}	0	−2.54 × 10^{-10}	−0.001	−2.01 × 10^{-10}
205	$C_7H_7(7) + C_7H_8O_3(42) \leftrightarrow$ toluene(1) + $C_7H_7O_3(39)$	0	−1.54 × 10^{-8}	0	−1.27 × 10^{-10}	−0.001	−1.05 × 10^{-10}
141	$C_7H_8O_2(16) + C_7H_7(7) \leftrightarrow$ toluene(1) + $C_7H_7O_2(12)$	0	−5.30 × 10^{-9}	0	−1.63 × 10^{-11}	0	−5.84 × 10^{-11}
145	$C_7H_7(7) + C_7H_8O_2(17) \leftrightarrow$ toluene(1) + $C_7H_7O_2(13)$	0	−5.30 × 10^{-9}	0	−1.63 × 10^{-11}	0	−5.57 × 10^{-11}
170	$C_7H_7(8) + C_7H_8O_2(15) \leftrightarrow$ toluene(1) + $C_7H_7O_2(27)$	0	1.85 × 10^{-17}	0	−1.56 × 10^{-18}	0	8.61 × 10^{-14}
175	$C_7H_7(9) + C_7H_8O_2(15) \leftrightarrow$ toluene(1) + $C_7H_7O_2(28)$	0	1.99 × 10^{-17}	0	−1.55 × 10^{-18}	0	8.68 × 10^{-14}
171	$C_7H_7(9) + C_7H_8O_2(15) \leftrightarrow$ toluene(1) + $C_7H_7O_2(27)$	0	2.46 × 10^{-13}	0	2.03 × 10^{-15}	0	8.69 × 10^{-14}
223	toluene(1) + $C_7H_5O(47)$ ↔ $C_7H_7(8)$ + $C_7H_6O(43)$	0	4.14 × 10^{-16}	0	3.40 × 10^{-18}	0	2.30 × 10^{-12}
176	toluene(1)+$C_7H_7O_2(28)$ ↔ $C_7H_7(10)$ + $C_7H_8O_2(15)$	0	−1.51 × 10^{-12}	0	−1.24 × 10^{-14}	0.001	3.15 × 10^{-12}
174	toluene(1) + $C_7H_7O_2(28)$ ↔ $C_7H_7(8)$ + $C_7H_8O_2(15)$	0	−2.46 × 10^{-13}	0	−2.03 × 10^{-15}	0.001	4.33 × 10^{-12}
178	toluene(1) + $C_7H_7O_2(29)$ ↔ $C_7H_7(8)$ + $C_7H_8O_2(15)$	0	2.85 × 10^{-12}	0	2.35 × 10^{-14}	0.001	4.49 × 10^{-12}
184	$C_7H_7(10) + C_7H_8O_2(15) \leftrightarrow$ toluene(1) + $C_7H_7O_2(30)$	0.2	8.10 × 10^{-8}	0.2	6.68 × 10^{-10}	0.199	1.21 × 10^{-9}
182	$C_7H_7(8) + C_7H_8O_2(15) \leftrightarrow$ toluene(1) + $C_7H_7O_2(30)$	0.4	1.62 × 10^{-7}	0.4	1.34 × 10^{-9}	0.398	2.42 × 10^{-9}
183	$C_7H_7(9) + C_7H_8O_2(15) \leftrightarrow$ toluene(1) + $C_7H_7O_2(30)$	0.4	1.62 × 10^{-7}	0.4	1.34 × 10^{-9}	0.4	2.43 × 10^{-9}

Table 12. Dominant Reactions in the Rate of Production of the Benzyl Radical at the Time of the Induction Period in the Mechanism, for the 433.15 K Temperature Criteria, Sorted by Rate for the Improved RMG Mechanism

| reaction number	reaction	core mechanism		extended mechanism		improved mechanism	
		fraction	mol cm^{-3} s^{-1}	fraction	mol cm^{-3} s^{-1}	fraction	mol cm^{-3} s^{-1}
9	$C_7H_7(7)$ + oxygen(2) ↔ $C_7H_7O_2(11)$	−1	−4.95 × 10^{-4}	−0.999	−2.24 × 10^{-6}	−0.999	−1.68 × 10^{-7}
2210	$C_7H_7(7)$ + $C_7H_7O_2(11)$ ↔ S(130)			−0.001	−1.9 × 10^{-9}	−0.001	−1.29 × 10^{-10}
17	HOOJ(5) + $C_7H_7(7)$ ↔ $C_7H_8O_2(15)$	0	−2.41 × 10^{-13}	0	−5.66 × 10^{-13}	0	−7.87 × 10^{-13}
145	$C_7H_7(7) + C_7H_8O_2(17) \leftrightarrow$ toluene(1) + $C_7H_7O_2(13)$	0	5.30 × 10^{-9}	0	1.63 × 10^{-11}	0	5.57 × 10^{-11}
141	$C_7H_8O_2(16) + C_7H_7(7) \leftrightarrow$ toluene(1) + $C_7H_7O_2(12)$	0	5.30 × 10^{-9}	0	1.63 × 10^{-11}	0	5.84 × 10^{-11}
131	toluene(1) + $C_7H_7(8)$↔toluene(1) + $C_7H_7(7)$	0	2.39 × 10^{-9}	0	1.99 × 10^{-11}	0	6.39 × 10^{-11}
132	toluene(1) + $C_7H_7(9)$ ↔ toluene(1) + $C_7H_7(7)$	0	2.39 × 10^{-9}	0	1.99 × 10^{-11}	0	6.41× 10^{-11}
205	$C_7H_7(7) + C_7H_8O_3(42) \leftrightarrow$ toluene(1) + $C_7H_7O_3(39)$	0	1.54 × 10^{-8}	0	1.27 × 10^{-10}	0.001	1.05 × 10^{-10}
197	$C_7H_7(7) + C_7H_8O_3(40) \leftrightarrow$ toluene(1) + $C_7H_7O_3(37)$	0	3.08 × 10^{-8}	0	2.54 × 10^{-10}	0.001	2.01 × 10^{-10}
165	$C_7H_7(7) + C_7H_8O(26) \leftrightarrow$ toluene(1) + $C_7H_7O(22)$	0	2.09 × 10^{-8}	0	1.74 × 10^{-10}	0.001	2.33 × 10^{-10}
201	$C_7H_7(7) + C_7H_8O_3(41) \leftrightarrow$ toluene(1) + $C_7H_7O_3(38)$	0	3.03 × 10^{-8}	0	2.46 × 10^{-10}	0.002	3.38 × 10^{-10}
278	$C_7H_7(7) + C_7H_8O_3(42) \leftrightarrow$ toluene(1) + $C_7H_7O_3(76)$	0	5.33 × 10^{-9}	0	4.77 × 10^{-11}	0.002	3.94 × 10^{-10}
161	$C_7H_7(7) + C_7H_8O(25) \leftrightarrow$ toluene(1) + $C_7H_7O(21)$	0	4.11 × 10^{-8}	0	3.37 × 10^{-10}	0.003	5.17 × 10^{-10}
157	$C_7H_7(7) + C_7H_8O(24) \leftrightarrow$ toluene(1) + $C_7H_7O(20)$	0	4.11 × 10^{-8}	0	3.38 × 10^{-10}	0.003	5.29 × 10^{-10}
127	toluene(1) + HOOJ(5) ↔ HOOH(6) + $C_7H_7(7)$	0	3.23 × 10^{-13}	0	1.67 × 10^{-10}	0.004	6.09 × 10^{-10}
250	$C_7H_7(7) + C_7H_8O_3(40) \leftrightarrow$ toluene(1) + $C_7H_7O_3(60)$	0	1.08 × 10^{-8}	0	9.64 × 10^{-11}	0.004	7.26 × 10^{-10}
274	$C_7H_7(7) + C_7H_8O_3(41) \leftrightarrow$ toluene(1) + $C_7H_7O_3(73)$	0	1.09 × 10^{-8}	0	9.76 × 10^{-11}	0.005	7.88 × 10^{-10}
153	toluene(1) + $C_7H_7O(19)$ ↔ $C_7H_7(7)$ + $C_7H_8O(23)$	0	1.35 × 10^{-9}	0.002	4.06 × 10^{-9}	0.016	2.74 × 10^{-9}
266	toluene(1) + $C_7H_5O_3(64)$ ↔ $C_7H_7(7)$ + $C_7H_6O_3(65)$	0.001	2.49 × 10^{-7}	0.001	2.10 × 10^{-9}	0.024	4.11 × 10^{-9}
123	toluene(1) + HOJ(3) ↔ $H_2O(4)$ + $C_7H_7(7)$	0.005	2.29 × 10^{-6}	0.008	1.89 × 10^{-8}	0.232	3.91 × 10^{-8}
137	$C_7H_7(7) + C_7H_8O_2(15) \leftrightarrow$ toluene(1) + $C_7H_7O_2(11)$	0.994	4.93 × 10^{-4}	0.988	2.22 × 10^{-6}	0.698	1.18 × 10^{-7}

highly reactive sites, which is reflected in the rate of production analysis, shown in Supplementary Tables 1 and 2. While the consumption of oxygen in the toluene mechanism at one induction period is centered only on the methyl group, shown in Table 11, the consumption of oxygen is dominant in the secondary carbons in the case of octane, shown in Supplementary Table 1.

4.4. Use of a Dedicated Low Temperature, Liquid Phase Condition Gas Phase Mechanism to Describe Liquid Phase Chemistry.

One question that is sometimes raised in the context of liquid phase chemistry is whether a gas phase mechanism may be adequate in describing the reaction system.[103,104] In the case where the overall mechanism is diffusion limited, it can be very safely concluded that a gas phase mechanism is inadequate for describing the chemistry of the system observed.[105−107] At the same time, the cage effect observed in the liquid phase may promote very specific reaction steps due to the initial products being constrained by the surrounding solvent.[108−110] In the gas phase, the products would instead have been more likely to separate without reacting further, which presents an additional complexity when discussing liquid phase kinetics.[108] Should a system be well mixed, or as is the case in the PetroOxy, provide a large surface area for the interaction of a thin film liquid test fuel with gaseous oxygen in the pressurized headspace, the details of the chemistry involved become less clear.[106,107]

For the case of the PetroOxy, it can be safely concluded that the oxidation process of toluene is limited by the kinetics of the reaction, as the oxygen consumption is over a magnitude slower when compared to other solvents. For example dodecane, a normal n-alkane, exhibits a residence time to a 10% pressure drop of roughly 75 min at 150 °C.[111] Thus, it can be concluded that in the specific case of the PetroOxy slowly oxidizing species are limited by the kinetics and not the gas to liquid transfer or the diffusion process within the liquid. It should be stressed that this does not suggest that diffusion has no effect, just that the process of oxygen consumption is dominated by the kinetics.

For comparison purposes, a gas phase mechanism targeting the liquid phase oxidation criteria for toluene was also created. Specifically, it targeted the 400−500 K temperature range, using an elevated pressure to simulate adequate concentrations. This is a methodology which is identical to the methodology applied to the chemical kinetics simulation, with the conditions previously given in Table 1. The same improvement steps as for the liquid phase mechanism are undertaken; i.e., the termination reactions are added and then the thermochemistry of the key species is updated. The observed behavior in the mechanism is extremely similar to that observed for the liquid phase, with minor differences that can only be determined in a direct comparison of the gas and liquid phase mechanisms. The corresponding induction period plot for the gas phase mechanism is shown in Figure 14. Concentration plots for the individual models are included in Supplementary Figures E.42, E.43, and E.44. Similarly to the liquid phase mechanism, the decomposition of the benzoyl radical is too rapid. For the sake of brevity, no detailed study of more appropriate parameters for the gas phase mechanism is undertaken and is left as a subject for future work. The associated mechanisms are included in Supplementary Section E.

It can further be noted that a mixing of thermodynamic parameters in reactions obtained for the liquid phase with a gas phase mechanism results in a behavior inconsistent with observed data as the energetics of reactions would be
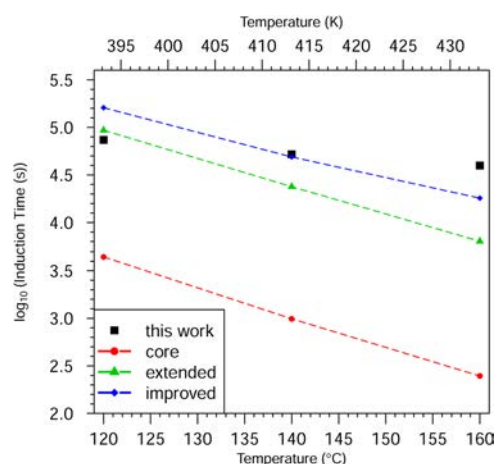
Figure 14. Plot of the logarithm of the induction time in seconds from the PetroOxy versus temperature. The gas phase versions of the core mechanism. The extended mechanism with added termination reactions and the improved mechanism with updated thermodynamic data using quantum chemistry calculations in ORCA are shown.[76]

unbalanced. Thus, it is important that mechanisms are designed using consistent rules, i.e., the entire mechanism being designed for the gas phase or the liquid phase using appropriate thermodynamic parameters but not a mix of both. For completion, comparative plots are shown in Supplementary Data Section E.6.

5. CONCLUSION & PERSPECTIVES FOR FUTURE WORK

This study uses an original methodology based on automated tools to develop a liquid phase detailed kinetic mechanism for toluene. The methodology combines an automated mechanism generator (RMG) that provides a skeletal detailed kinetic mechanism and theoretical calculations to update the thermodynamic data of key species. Induction periods at three temperatures and species profiles obtained using a PetroOxy apparatus, as well as gas chromatography coupled to a flame ionization detector and mass spectrometry are used to validate the model.

The final mechanism generated consists of 173 species and 2309 reactions. A replacement of the estimated thermodynamic data with the aid of quantum chemistry calculations at the DFT level for 32 key species has resulted in a fairly significant improvement in the qualitative behavior of the model compared to the raw mechanism developed with RMG. The major routes identified in the literature involving the formation of benzyl alcohol and benzaldehyde are present, and the mechanism reproduces the expected overall behavior of a larger concentration of benzaldehyde compared to benzyl alcohol fairly well. The quantitative agreement of the model with the experimental induction period also improved as a result of the updates to the thermodynamic parameters. A comparison with the measured toluene species profile further highlights the capability of the mechanism.

However, a discrepancy remains in the induction period prediction with the final model. Updates to the thermodynamic parameters are insufficient to obtain a good agreement between available experimental data for the temperature dependence of the model. The model exhibits a reactivity that is too slow by approximately 0.6 orders of magnitude relative to the experimental induction period at 120 °C (393.15 K), while

exhibiting a reactivity that is too fast by around 0.2 orders of magnitude relative to the experimental induction period at 160 °C (433.15 K). Sensitivity analysis suggests that the kinetic parameters only have a small impact on the temperature dependence of the model with regard to the induction period. Further improvements are hence likely to come from either a more extensive study into thermodynamic parameters using more accurate quantum chemistry methods or by the inclusion of additional pathways that were not considered by RMG. While beyond the scope of this work, it may be interesting to study the constituents of the mechanism with fast high accuracy methods, such as local-pair-natural-orbital based methods.[112,113] The use of explicit solvation possibly using molecular dynamics simulations could also offer the opportunity to obtain more accurate thermodynamic parameters for the involved species in solution.[72]

Another area that offers opportunities for future work is an implementation of the gas to liquid transfer, potentially taking the headspace gas phase chemistry into account, which will allow for a more realistic modeling of the system. Currently the model is assessed under the assumption that the oxygen concentration is constant, which is only applicable toward the beginning of the experiment. Gradual consumption of oxygen in the headspace will invariably reduce the oxygen concentration in the liquid phase, which needs to be considered by the solver, which for the PetroOxy may be described using a comparatively simple relationship.[111]

Experimental work to establish a reliable reproducible method by which toluene which is thermally stressed in a batch reactor as well as the resultant products can be analyzed both qualitatively and quantitatively is currently the subject of ongoing research at IFPEN and will be the subject of a future publication. Such data can then be used to further assess the quality of the model and aid in the implementation of further improvements where required.

Finally, toluene as an aromatic is an essential compound in fuel formulation that provides high octane number, seal swell, and lubrication for jet fuels. As a precursor of particulate matter in the gas phase, it has been shown that aromatics are also implicated in deposit formation in the liquid phase. Such a detailed kinetic mechanism is thus of interest when considering fuel design to optimize its properties while preventing any side effects. The mechanism provides a relevant working basis for further investigations on the nonlinear behavior of more complex fuel mixtures' co-oxidation. It can also be of interest for simulating fuel additives in the liquid phase following the addition of the required submechanisms.

ASSOCIATED CONTENT

Ⓢ Supporting Information

The Supporting Information is available free of charge on the ACS Publications website at DOI: 10.1021/acs.energy-fuels.7b00416.

> General supplementary data, PetroOxy data, quantum chemistry related supplementary data, liquid phase chemical kinetics mechanisms, gas phase chemical kinetics mechanisms for liquid phase conditions (PDF)

AUTHOR INFORMATION

Corresponding Author

*E-mail: mickael.matrat@ifpen.fr.

ORCID

Detlev Conrad Mielczarek: 0000-0002-4720-353X

Notes

The authors declare no competing financial interest.

REFERENCES

(1) Hoorn, J.; Alsters, P.; Versteeg, G. A Kinetic Model for Toluene Oxidation Comprising Benzylperoxy Benzoate Ester as Reactive Intermediate in the Formation of Benzaldehyde. *Int. J. Chem. React. Eng.* **2005**, *3*, 1−19.

(2) Hermans, I.; Peeters, J.; Vereecken, L.; Jacobs, P. A. Mechanism of Thermal Toluene Autoxidation. *ChemPhysChem* **2007**, *8*, 2678−2688.

(3) Hemighaus, G.; Boval, T.; Bacha, J. D.; Barnes, F.; Franklin, M.; Gibbs, L.; Hogue, N.; Jones, J.; Lesnini, D.; Lind, J.; Morris, J. *Aviation Fuels Techn. Rev.*, 2006.

(4) Corporan, E.; Edwards, T.; Shafer, L. M.; DeWitt, M. J.; Klingshirn, C.; Zabarnick, S.; West, Z. J.; Striebich, R. C.; Graham, J.; Klein, J. Chemical, Thermal Stability, Seal Swell, and Emissions Studies of Alternative Jet Fuels. *Energy Fuels* **2011**, *25*, 955−966.

(5) Sicard, M.; Hein, C.; Gernigon, S.; Ser, F.; Brodzki, D.; Djega-mariadassou, G. Study of the Oxidation of the Main Hydrocarbon Families Contained in the Kerosene Jet A-1. 10th International Conference on Stability, Handling and Use of Liquid Fuels, Tuscon, Arizona, 2007, pp 1−20

(6) Rye, L. J.; Blakey, S.; Wilson, C. W. Sustainability of supply or the planet: a review of potential drop-in alternative aviation fuels. *Energy Environ. Sci.* **2010**, *3*, 17.

(7) Edwards, T. Cracking and Deposition Behaviour of Supercritical Hydrocarbon Aviation Fuels. *Combust. Sci. Technol.* **2006**, 307−334.

(8) Jones, E. G.; Balster, L. M.; Balster, W. J. Thermal Stability of Jet-A Fuel Blends. *Energy Fuels* **1996**, *10*, 509−515.

(9) Balster, L. M.; Zabarnick, S.; Striebich, R. C.; Shafer, L. M.; West, Z. J. Analysis of polar species in jet fuel and determination of their role in autoxidative deposit formation. *Energy Fuels* **2006**, *20*, 2564−2571.

(10) Naik, C. V.; Pitz, W. J.; Sjöberg, M.; Dec, J. E.; Orme, J.; Curran, H. J.; Simmie, J. M.; Westbrook, C. K. Detailed Chemical Kinetic Modeling of Surrogate Fuels for Gasoline and Application to an HCCI Engine. 2005 Joint Meeting of the U.S. Sections of The Combustion Institute, 2005.

(11) Andrae, J. C. G. Comprehensive chemical kinetic modeling of toluene reference fuels oxidation. *Fuel* **2013**, *107*, 740−748.

(12) Ervin, J. S.; Zabarnick, S. Computational fluid dynamics simulations of jet fuel oxidation incorporating pseudo-detailed chemical kinetics. *Energy Fuels* **1998**, *12*, 344−352.

(13) Kuprowicz, N. J.; Zabarnick, S.; West, Z. J.; Ervin, J. S. Use of Measured Species Class Concentrations with Chemical Kinetic Modeling for the Prediction of Autoxidation and Deposition of Jet Fuels. *Energy Fuels* **2007**, *21*, 530−544.

(14) Westbrook, C. K.; Pitz, W. J.; Herbinet, O.; Curran, H. J.; Silke, E. J. A comprehensive detailed chemical kinetic reaction mechanism for combustion of n-alkane hydrocarbons from n-octane to n-hexadecane. *Combust. Flame* **2009**, *156*, 181−199.

(15) Ben Amara, A.; Nicolle, A.; Alves-Fortunato, M.; Jeuland, N. Toward Predictive Modeling of Petroleum and Biobased Fuel Stability: Kinetics of Methyl Oleate/n-Dodecane Autoxidation. *Energy Fuels* **2013**, *27*, 6125−6133.

(16) Chatelain, K.; Nicolle, A.; Ben Amara, A.; Catoire, L.; Starck, L. Wide Range Experimental and Kinetic Modeling Study of Chain Length Impact on n-Alkanes Autoxidation. *Energy Fuels* **2016**, *30*, 1294−1303.

(17) Van De Vijver, R.; Vandewiele, N. M.; Bhoorasingh, P. L.; Slakman, B. L.; Khanshan, F. S.; Carstensen, H. H.; Reyniers, M. F.; Marin, G. B.; West, R. H.; Van Geem, K. M. Automatic mechanism and kinetic model generation for gas- And solutionphase processes: A perspective on best practices, recent advances, and future challenges. *Int. J. Chem. Kinet.* **2015**, *47*, 199−231.

(18) Benson, S. W.; Cruickshank, F. R.; Golden, D. M.; Haugen, G. R.; O'Neal, H. E.; Rodgers, A. S.; Shaw, R.; Walsh, R. Additivity rules for the estimation of thermochemical properties. *Chem. Rev.* **1969**, *69*, 279−324.

(19) Warth, V.; Battin-Leclerc, F.; Fournet, R.; Glaude, P.-J.; Come, G.; Scacchi, G. Computer based generation of reaction mechanisms for gas-phase oxidation. *Comput. Chem.* **2000**, *24*, 541−60.

(20) Touchard, S.; Fournet, R.; Glaude, P. A.; Warth, V.; Battin-Leclerc, F.; Vanhove, G.; Ribaucour, M.; Minetti, R. Modeling of the oxidation of large alkenes at low temperature. *Proc. Combust. Inst.* **2005**, *30*, 1073−1080.

(21) Biet, J.; Hakka, M. H.; Warth, V.; Glaude, P. A.; Battin-Leclerc, F. Experimental and modeling study of the low-temperature oxidation of large alkanes. *Energy Fuels* **2008**, *22*, 2258−2269.

(22) Vandewiele, N. M.; Van Geem, K. M.; Reyniers, M.-F.; Marin, G. B. Genesys: Kinetic model construction using chemo-informatics. *Chem. Eng. J.* **2012**, *207−208*, 526−538.

(23) Gao, C. W.; Allen, J. W.; Green, W. H.; West, R. H. Reaction Mechanism Generator: Automatic construction of hemical kinetic mechanisms. *Comput. Phys. Commun.* **2016**, *203*, 212−225.

(24) Anton Paar GmbH, PetroOxy Manual, 2013.

(25) Ben Amara, A.; Kaoubi, S.; Starck, L. Toward an optimal formulation of alternative jet fuels: Enhanced oxidation and thermal stability by the addition of cyclic molecules. *Fuel* **2016**, *173*, 98−105.

(26) Van Geem, K. M.; Reyniers, M.-F.; Marin, G. B.; Song, J.; Green, W. H.; Matheu, D. M. Automatic reaction network generation using RMG for steam cracking of n-hexane. *AIChE J.* **2006**, *52*, 718−730.

(27) Vandewiele, N. M.; Magoon, G. R.; Van Geem, K. M.; Green, W. H.; Marin, G. B.; Reyniers, M.-F. Experimental and Modeling Study on the Thermal Decomposition of Jet Propellant-10. *Energy Fuels* **2014**, *28*, 4976.

(28) Green, W. H. et al. *RMG - Reaction Mechanism Generator v4.0*, 2013.

(29) Jalan, A.; West, R. H.; Green, W. H. An Extensible Framework for Capturing Solvent Effects in Computer Generated Kinetic Models. *J. Phys. Chem. B* **2013**, *117*, 2955.

(30) Jalan, A.; Ashcraft, R. W.; West, R. H.; Green, W. H. Predicting solvation energies for kinetic modeling. *Annu. Rep. Prog. Chem., Sect. C: Phys. Chem.* **2010**, *106*, 211.

(31) Taft, R. W.; Abboud, J.-L. M.; Kamlet, M. J.; Abraham, M. Linear solvation energy relations. *J. Solution Chem.* **1985**, *14*, 153−186.

(32) Abraham, M. H.; Platts, J. A.; Hersey, A.; Leo, A. J.; Taft, R. W. Correlation and Estimation of Gas - Chloroform and Water -

Chloroform Partition Coefficients by a Linear Free Energy Relation-ship Method. *J. Pharm. Sci.* **1999**, *88*, 670.

(33) Mintz, C.; Clark, M.; Acree, W. E.; Abraham, M. H. Enthalpy of Solvation Corrections for Gaseous Solutes Dissolved in Water and in 1-Octanol Based on the Abraham Model. *J. Chem. Inf. Model.* **2007**, *47*, 115−121.

(34) Mintz, C.; Clark, M.; Burton, K.; Acree, W. E.; Abraham, M. H. Enthalpy of Solvation Correlations for Gaseous Solutes Dissolved in Toluene and Carbon Tetrachloride Based on the Abraham Model. *J. Solution Chem.* **2007**, *36*, 947−966.

(35) Mintz, C.; Burton, K.; Acree, W.; Abraham, M. H. Enthalpy of Solvation Correlations For Gaseous Solutes Dissolved in Linear Alkanes (C5-C16) Based on the Abraham Model. *QSAR Comb. Sci.* **2008**, *27*, 179−186.

(36) Mintz, C. Predicting Chemical and Biochemical Properties using the Abraham General Solvation Model. Ph.D. thesis, University of North Texas, 2009.

(37) The RMG-Py Developers, http://reactionmechanismgenerator.github.io/RMG-Py/users/rmg/Liquids.html, Accessed 18th July 2016.

(38) Bamford, C.H.; C, T.; Compton, R., Eds. *Diffusion-Limited Reactions*; Comprehensive Chemical Kinetics; Elsevier, 1985; Vol. 25.

(39) West, R. https://github.com/ReactionMechanismGenerator/RMG-Py/commit/bd96765dafa1e7e1eb38a9ffcf1bd1bfd8fbf2a6, Accessed 5th January 2017.

(40) Goerigk, L.; Grimme, S. Efficient and accurate double-hybrid-meta-GGA density functionals- evaluation with the extended GMTKN30 database for general main group thermochemistry, kinetics, and noncovalent interactions. *J. Chem. Theory Comput.* **2011**, *7*, 291−309.

(41) Frisch, M. J. et al.. *Gaussian 09*, Revision E.01; Gaussian Inc.: Wallingford CT, 2009.

(42) Sandhiya, L.; Zipse, H. Initiation Chemistries in Hydrocarbon (Aut)Oxidation. *Chem. - Eur. J.* **2015**, *21*, 14060−14067.

(43) Martin, J. M. L.; de Oliveira, G. Towards standard methods for benchmark quality ab initio thermochemistry—W1 and W2 theory. *J. Chem. Phys.* **1999**, *111*, 1843−1856.

(44) Somers, K. P.; Simmie, J. M. Benchmarking Compound Methods (CBS-QB3, CBSAPNO, G3, G4, W1BD) against the Active Thermochemical Tables: Formation Enthalpies of Radicals. *J. Phys. Chem. A* **2015**, *119*, 8922−8933.

(45) Karton, A.; Goerigk, L. Accurate reaction barrier heights of pericyclic reactions: Surprisingly large deviations for the CBS-QB3 composite method and their consequences in DFT benchmark studies. *J. Comput. Chem.* **2015**, *36*, 622−632.

(46) Karton, A.; Gruzman, D.; Martin, J. M. L. Benchmark thermochemistry of the CnH2n+2 alkane isomers (n = 2−8) and performance of DFT and composite ab initio methods for dispersion-driven isomeric equilibria. *J. Phys. Chem. A* **2009**, *113*, 8434−8447.

(47) Foresman, J. B.; Frisch, A. Exploring Chemistry With Electronic Structure Methods, 1996.

(48) Yu, H. S.; Li, S. L.; Truhlar, D. G. Perspective: Kohn-Sham density functional theory descending a staircase. *J. Chem. Phys.* **2016**, *145*, 130901.

(49) Zabarnick, S.; Phelps, D. K. Density Functional Theory Calculations of the Energetics and Kinetics of Jet Fuel Autoxidation Reactions. *Energy Fuels* **2006**, *20*, 488−497.

(50) Osmont, A.; Catoire, L.; Gökalp, I.; Yang, V. Ab initio quantum chemical predictions of enthalpies of formation, heat capacities, and entropies of gas-phase energetic compounds. *Combust. Flame* **2007**, *151*, 262−273.

(51) da Silva, G.; Rafiq Hamdan, M.; Bozzelli, J. W. Oxidation of the benzyl radical: Mechanism, thermochemistry, and kinetics for the reactions of benzyl hydroperoxide. *J. Chem. Theory Comput.* **2009**, *5*, 3185−3194.

(52) Zhang, I. Y.; Wu, J.; Xu, X. Extending the reliability and applicability of B3LYP. *Chem. Commun. (Cambridge, U. K.)* **2010**, *46*, 3057−3070.

(53) Kruse, H.; Goerigk, L.; Grimme, S. Why the standard B3LYP/6-31G* model chemistry should not be used in DFT calculations of

molecular thermochemistry: Understanding and correcting the problem. *J. Org. Chem.* **2012**, *77*, 10824−10834.

(54) Grimme, S. Seemingly simple stereoelectronic effects in alkane isomers and the implications for Kohn-Sham density functional theory. *Angew. Chem., Int. Ed.* **2006**, *45*, 4460−4464.

(55) Wodrich, M. D.; Corminboeuf, C.; Schleyer, P. V. R. Systematic errors in computed alkane energies using B3LYP and other popular DFT functionals. *Org. Lett.* **2006**, *8*, 3631−3634.

(56) Schreiner, P. R. Relative energy computations with approximate density functional theory - A caveat! *Angew. Chem., Int. Ed.* **2007**, *46*, 4217−4219.

(57) Wodrich, M. D.; Corminboeuf, C.; Schreiner, P. R.; Fokin, A. A.; Von Rague Schleyer, P. How accurate are DFT treatments of organic energies? *Org. Lett.* **2007**, *9*, 1851−1854.

(58) Zhao, Y.; Truhlar, D. G. How well can new-generation density functionals describe the energetics of bond-dissociation reactions producing radicals? *J. Phys. Chem. A* **2008**, *112*, 1095−1099.

(59) Steinmann, S. N.; Wodrich, M. D.; Corminboeuf, C. Overcoming systematic DFT errors for hydrocarbon reaction energies. *Theor. Chem. Acc.* **2010**, *127*, 429−442.

(60) Cohen, A. J.; Mori-Śanchez, P.; Yang, W. Challenges for Density Functional Theory. *Chem. Rev.* **2012**, *112*, 289−320.

(61) Tirado-Rives, J.; Jorgensen, W. L. Performance of B3LYP density functional methods for a large set of organic molecules. *J. Chem. Theory Comput.* **2008**, *4*, 297−306.

(62) Zhao, Y.; Truhlar, D. G. The M06 suite of density functionals for main group thermochemistry, thermochemical kinetics, non-covalent interactions, excited states, and transition elements: Two new functionals and systematic testing of four M06-class functionals and 12 other function. *Theor. Chem. Acc.* **2008**, *120*, 215−241.

(63) Zhao, Y.; Truhlar, D. G. Applications and validations of the Minnesota density functionals. *Chem. Phys. Lett.* **2011**, *502*, 1−13.

(64) Rokob, T. A.; Hamza, A.; Papai, I. Pápai, I. Computing reliable energetics for conjugate addition reactions. *Org. Lett.* **2007**, *9*, 4279−4282.

(65) Peverati, R.; Truhlar, D. G. Quest for a universal density functional: the accuracy of density functionals across a broad spectrum of databases in chemistry and physics. *Philos. Trans. R. Soc., A* **2014**, *372*, 20120476.

(66) Weigend, F.; Ahlrichs, R. Balanced basis sets of split valence, triple zeta valence and quadruple zeta valence quality for H to Rn: Design and assessment of accuracy. *Phys. Chem. Chem. Phys.* **2005**, *7*, 3297−3305.

(67) Weigend, F. Accurate Coulomb-fitting basis sets for H to Rn. *Phys. Chem. Chem. Phys.* **2006**, *8*, 1057−1065.

(68) Goerigk, L.; Grimme, S. A thorough benchmark of density functional methods for general main group thermochemistry, kinetics, and noncovalent interactions. *Phys. Chem. Chem. Phys.* **2011**, *13*, 6670−6688.

(69) Marenich, A. V.; Cramer, C. J.; Truhlar, D. G. Universal Solvation Model Based on Solute Electron Density and on a Continuum Model of the Solvent Defined by the Bulk Dielectric Constant and Atomic Surface Tensions. *J. Phys. Chem. B* **2009**, *113*, 6378−6396.

(70) Sure, R.; Grimme, S. Comprehensive Benchmark of Association (Free) Energies of Realistic Host-Guest Complexes. *J. Chem. Theory Comput.* **2015**, *11*, 3785−3801.

(71) Guerard, J. J.; Arey, J. S. Critical evaluation of implicit solvent models for predicting aqueous oxidation potentials of neutral organic compounds. *J. Chem. Theory Comput.* **2013**, *9*, 5046−5058.

(72) Velez-Vega, C.; McKay, D. J. J.; Kurtzman, T.; Aravamuthan, V.; Pearlstein, R. A.; Duca, J. S. Estimation of Solvation Entropy and Enthalpy via Analysis of Water Oxygen-Hydrogen Correlations. *J. Chem. Theory Comput.* **2015**, *11*, 5090−5102.

(73) Denisov, E. T.; Afanas'ev, I. B. *Oxidation and Antioxidants in Organic Chemistry and Biology*; Taylor & Francis, 2005.

(74) Atkins, P.; de Paula, J. *Physical Chemistry*, 8th ed.; W. H. Freeman and Company, 2011.

(75) Ervin, J. S.; Williams, T. F. Dissolved oxygen concentration and jet fuel deposition. *Ind. Eng. Chem. Res.* **1996**, *35*, 899−904.

(76) Neese, F. The ORCA program system. *Wiley Interdisciplinary Reviews: Computational Molecular Science* **2012**, *2*, 73−78.

(77) Burgess, D. *NIST Chemistry WebBook, NIST Standard Reference Database Number 69* ; National Institute of Standards and Technology: Gaithersburg, MD, 20899.

(78) Ponomarev, D. A.; Takhistov, V. V. What are Isodesmic Reactions? *J. Chem. Educ.* **1997**, *74*, 201.

(79) Bakowies, D. Ab initio thermochemistry using optimal-balance models with isodesmic corrections: The ATOMIC protocol. *J. Chem. Phys.* **2009**, *130*, 144113.

(80) Arnason, I.; Gudnason, P. I.; Björnsson, R.; Oberhammer, H. Gas Phase Structures, Energetics, and Potential Energy Surfaces of. *J. Phys. Chem. A* **2011**, *115*, 10000−10008.

(81) Saraf, S. R.; Rogers, W. J.; Mannan, M. S.; Hall, M. B.; Thomson, L. M. Theoretical thermochemistry: Ab initio heat of formation for hydroxylamine. *J. Phys. Chem. A* **2003**, *107*, 1077−1081.

(82) Cramer, C. J. *Essentials of Computational Chemistry*; Wiley, 2004; pp 334−342.

(83) Snitsiriwat, S.; Bozzelli, J. W. Thermochemistry, Reaction Paths, and Kinetics on the tert-Isooctane Radical Reaction with O2. *J. Phys. Chem. A* **2014**, *118*, 4631.

(84) Tange, O. GNU Parallel - The Command-Line Power Tool. *login: The USENIX Magazine* **2011**, *36*, 42−47.

(85) R Core Team, R.: *A Language and Environment for Statistical Computing*, R Foundation for Statistical Computing: Vienna, Austria, 2016.

(86) Bacha, K.; Ben Amara, A.; Vannier, A.; Alves-Fortunato, M.; Nardin, M. Oxidation stability of diesel/biodiesel fuels measured by PetroOxy device and characterization of oxidation products. *Energy Fuels* **2015**, *29*, 4345.

(87) Wenig, P.; Odermatt, J. OpenChrom: a cross-platform open source software for the mass spectrometric analysis of chromatographic data. *BMC Bioinf.* **2010**, *11*, 405.

(88) Wenig, P. Post-optimization of Py-GC/MS data: A case study using a new digital chemical noise reduction filter (NOISERA) to enhance the data quality utilizing OpenChrom mass spectrometric software. *J. Anal. Appl. Pyrolysis* **2011**, *92*, 202−208.

(89) Murphy, K. R.; Wenig, P.; Parcsi, G.; Skov, T.; Stuetz, R. M. Characterizing odorous emissions using new software for identifying peaks in chemometric models of gas chromatography−mass spectrometry datasets. *Chemom. Intell. Lab. Syst.* **2012**, *118*, 41−50.

(90) Hoorn, J. a. a.; Van Soolingen, J.; Versteeg, G. F. Modeling toluene oxidation: Incorporation of Mass Transfer Phenomena. *Chem. Eng. Res. Des.* **2005**, *83*, 187−195.

(91) Tan, P.; Tang, S.; Liang, B. Kinetic Models for Liquid-Phase Catalytic Oxidation of Toluene To Benzoic Acid With Pure Oxygen. *Chem. Eng. Commun.* **2010**, *197*, 953−962.

(92) Kantam, M. L.; Sreekanth, P.; Rao, K. K.; Kumar, T. P.; Rao, B. P. C.; Choudary, B. M. An improved process for selective liquid-phase air oxidation of toluene. *Catal. Lett.* **2002**, *81*, 223−232.

(93) Rolland, S.; Simmie, J. M. The comparison of detailed chemical kinetic mechanisms; forward versus reverse rates with CHEMRev. *Int. J. Chem. Kinet.* **2005**, *37*, 119−125.

(94) Nozaki, K.; Bartlett, P. D. The Kinetics of Decomposition of Benzoyl Peroxide in Solvents. I. *J. Am. Chem. Soc.* **1946**, *68*, 1686−1692.

(95) Barnett, B.; Vaughan, W. E. The Decomposition of Benzoyl Peroxide. II. The Rates of Decomposition in Various Solvents. *J. Phys. Colloid Chem.* **1947**, *51*, 942−955.

(96) Barson, C.; Bevington, J. A tracer study of the benzoyloxy radical. *Tetrahedron* **1958**, *4*, 147−156.

(97) Radziszewski, J. G.; Nimlos, M. R.; Winter, P. R.; Ellison, G. B. Infrared Absorption Spectroscopy of the Phenyl Radical. *J. Am. Chem. Soc.* **1996**, *118*, 7400−7401.

(98) Brown, D. J. The Thermal Decomposition of Benzoyl Peroxide. *J. Am. Chem. Soc.* **1940**, *62*, 2657−2659.

(99) Blake, P.; Jackson, G. The thermal decomposition of acetic acid. *J. Chem. Soc. B* **1968**, 1153−1155.

(100) Lehni, M.; Schuh, H.; Fischer, H. Rate Constants for the Termination of Benzyl Radicals in Solution. *Int. J. Chem. Kinet.* **1979**, *11*, 705−713.

(101) Battino, R.; Rettich, T. T.; Tominaga, T. The Solubility of Oxygen and Ozone in Liquids. *J. Phys. Chem. Ref. Data* **1983**, *12*, 163−178.

(102) Li, A.; Tang, S.; Tan, P.; Liu, C.; Liang, B. Measurement and prediction of oxygen solubility in toluene at temperatures from 298.45 to 393.15 K and pressures up to 1.0 MPa. *J. Chem. Eng. Data* **2007**, *52*, 2339−2344.

(103) Patrick, C. R. Reactions in the gas and liquid phases: Comparison of kinetic and thermodynamic data. *Int. J. Chem. Kinet.* **1973**, *5*, 769−776.

(104) Mayo, F. R. Comparison of liquid-phase and gas-phase reactions of free radicals. *J. Am. Chem. Soc.* **1967**, *89*, 2654−2661.

(105) Rice, S. *Diffusion-Limited Reactions*; Comprehensive Chemical Kinetics; Elsevier Science, 1985.

(106) van Krevelen, D. W.; Hoftijzer, P. J. Kinetics of gas-liquid reactions part I. General theory. *Recueil des Travaux Chimiques des Pays-Bas* **1948**, *67*, 563−586.

(107) Nathanson, G. M.; Davidovits, P.; Worsnop, D. R.; Kolb, C. E. Dynamics and Kinetics at the Gas-Liquid Interface. *J. Phys. Chem.* **1996**, *100*, 13007−13020.

(108) Franck, J.; Rabinowitsch, E. Some remarks about free radicals and the photochemistry of solutions. *Trans. Faraday Soc.* **1934**, *30*, 120−130.

(109) Patron, F.; Adelman, S. A. Solvent cage effects and chemical dynamics in liquids. *Chem. Phys.* **1991**, *152*, 121−131.

(110) Braden, D. A.; Parrack, E. E.; Tyler, D. R. Solvent cage effects. I. Effect of radical mass and size on radical cage pair recombination efficiency. II. Is geminate recombination of polar radicals sensitive to solvent polarity? *Coord. Chem. Rev.* **2001**, *211*, 279−294.

(111) Mielczarek, D. C. Autoxidation Behaviour of Hydrocarbons in the Context of Conventional and Alternative Aviation Fuels. Ph.D. thesis, School of Chemical and Process Engineering, University of Leeds, 2015; uk.bl.ethos.668749.

(112) Liakos, D. G.; Neese, F. Is It Possible to Obtain Coupled Cluster Quality Energies at near Density Functional Theory Cost? Domain-Based Local Pair Natural Orbital Coupled Cluster vs Modern Density Functional Theory. *J. Chem. Theory Comput.* **2015**, *11*, 4054−4063.

(113) Paulechka, E.; Kazakov, A. Efficient DLPNO−CCSD(T)-Based Estimation of Formation Enthalpies for C-, H-, O-, and N-Containing Closed-Shell Compounds Validated Against Critically Evaluated Experimental Data. *J. Phys. Chem. A* **2017**, *121*, 4379.